Mitochondrial oxidative stress-mediated ferroptosis as a contributing factor of refrigerated beef tenderness: from mitochondrial biochemistry and proteomics perspective

Ningxia Bu, Qi Yang, Weihua Liu, Jun Liu, Anran Zheng, Yao Zhang, Dunhua Liu

PII: S2212-4292(24)01054-X

DOI: https://doi.org/10.1016/j.fbio.2024.104624

Reference: FBIO 104624

To appear in: *Food Bioscience*

Received Date: 27 March 2024

Revised Date: 12 May 2024

Accepted Date: 21 June 2024

Please cite this article as: Bu N., Yang Q., Liu W., Liu J., Zheng A., Zhang Y. & Liu D., Mitochondrial oxidative stress-mediated ferroptosis as a contributing factor of refrigerated beef tenderness: from mitochondrial biochemistry and proteomics perspective, *Food Bioscience*, https://doi.org/10.1016/j.fbio.2024.104624.

Graphical abstract

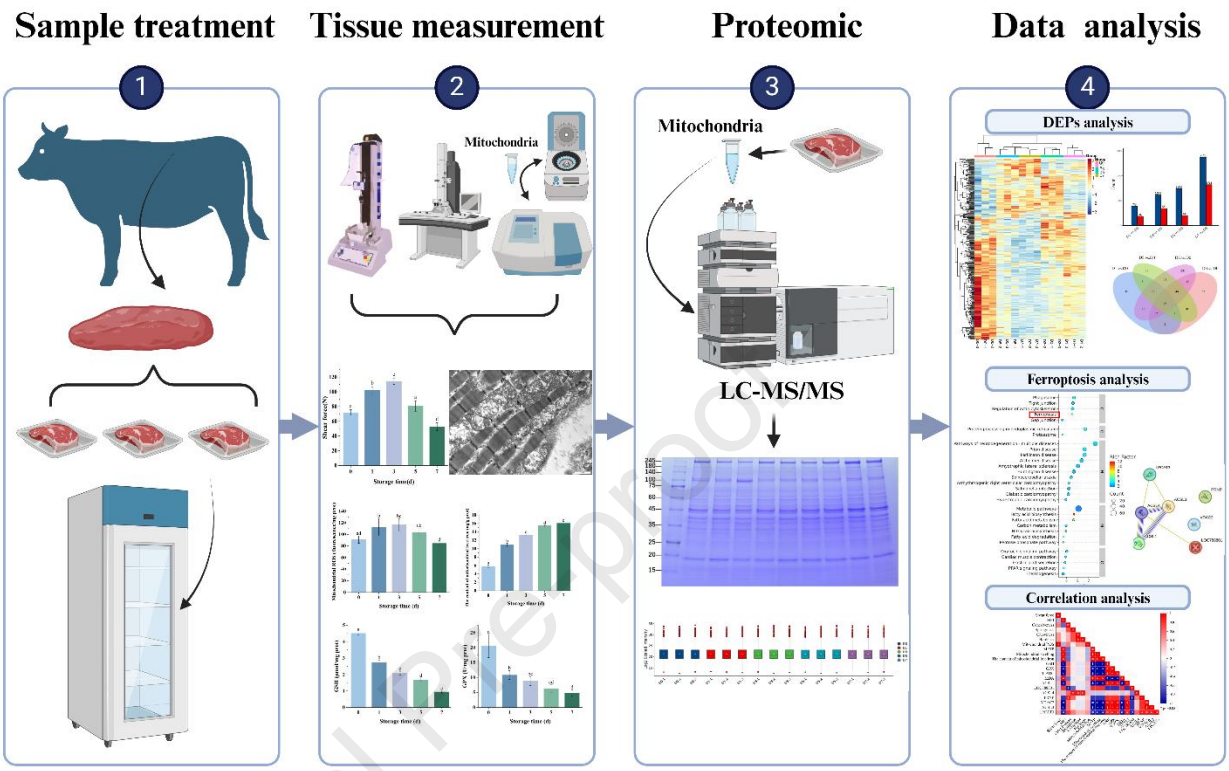

Mitochondrial oxidative stress-mediated ferroptosis as a contributing factor of refrigerated beef tenderness: from mitochondrial biochemistry and proteomics perspective

Ningxia Bu [a], Qi Yang [b], Weihua Liu [b], Jun Liu [c], Anran Zheng [a], Yao Zhang [a] and Dunhua Liu [a, d *]

[a] College of Animal Science and Technology, Ningxia University, 750021, Yinchuan, PR China

[b] Ningxia Veterinary Drugs and Fodder Inspection Institute, 750011, Yinchuan, PR China

[c] School of Life Sciences, Hubei Normal University, 435002, Huangshi, PR China

[d] College of Food Science and Engineering, Ningxia University, 750021, Yinchuan, PR China

* Corresponding author: Professor Dunhua Liu

Corresponding author at: No.489, Mount Helan West Road, Xixia District, Yinchuan City, 750000, Ningxia, China.

E-mail addresses: ldh320@nxu.edu.cn (D. Liu).

Tel.: +86-13995288707

Abstract: This study aimed to investigate the mechanism of ferroptosis mediated by mitochondrial oxidative stress and its potential associations with tenderness of beef during refrigeration. Results showed that mitochondrial reactive oxygen species (ROS) reached a maximum at day 3 (116.67±8.50 mg protein), the degree of mitochondrial swelling, mitochondrial membrane permeability increased with the increase of refrigeration time, and mitochondrial free iron content increased significantly (p<0.05), while mitochondria showed the morphological features of ferroptosis. In addition, the decreased levels of reduced glutathione, total antioxidant capacity and the activity of glutathione peroxidase, and the accumulation of malondialdehyde reflected an imbalance in mitochondrial antioxidant defense system, presenting the physiological characteristics of ferroptosis. Furthermore, mitochondrial TMT quantitative proteomics identified 7 differentially expressed proteins (DEPs) enriched to the ferroptosis pathway, including ACSL1, LOC788801, ACSL4, PRNP, VDAC2, ACSL3 and LPCAT3, which were primarily involved in lipid metabolism pathway and were the major mitochondrial pathway involved in ferroptosis during beef refrigeration. Besides, ROS and lipid peroxidation from mitochondrial oxidative stress-mediated ferroptosis attacked tissue myofibril structure and increased myofibrillar fragmentation index, which promoted the improvement of postmortem meat tenderness. These findings provided new perspectives on the role of mitochondria in cell death and the effect of ferroptosis on muscle tenderization.

Keywords: Mitochondria, Ferroptosis, Oxidative stress, Tenderness, Beef

1. Introduction

Beef is one of the most widely consumed meats in the world, with increasing global consumption due to its high nutritional quality, including dietary proteins, minerals and vitamins required for physiological processes and development of the human body (Eva et al., 2022; Yirenkyiwaa et al., 2022). According to Food and Agriculture Organization (FAO), the global production of beef in 2022 was about 5.29 million metric tons with a 10-year growth rate of 3%. In recent years, with the continuous improvement of peoples living standards, meat demand has entered an era of quantity and quality coexistence, research on beef quality control and improvement has gradually become a hot topic (Machestropa et al., 2024; Wang et al., 2023). The quality of beef is an essential factor influencing consumer's preference and market acceptance, including texture, tenderness, flavour, color and juiciness, with tenderness as a crucial indicator for beef overall palatability (Iliani et al., 2024). Postmortem muscle-to-meat conversion is a complex biological process accompanied by changes in tenderness. Recent studies suggested that meat tenderness was closely linked to multiple types of muscle cell death, including autophagy, apoptosis, pyroptosis and necrosis (Liu et al., 2023; Chen et al., 2020). Mitochondria are considered to be an aggregation point for the cell death signals (Huang et al., 2023), postmortem skeletal muscle is rapidly placed in a state of ischemia and hypoxia, and mitochondria are the earliest organelles to be affected, leading to oxidative stress, mitochondrial dysfunction, and cell death as a result of impaired antioxidant defense system and excessive reactive oxygen species (ROS) production (Peoples et al., 2019). ROS are unstable molecules produced mainly by mitochondria,

such as superoxide anion radical, hydroxyl radicals, singlet oxygen and hydrogen peroxide, which can act as signaling molecules involved in the oxidative stress process in cells and induce apoptosis and damage muscle tissues (Hekimi et al., 2016), It was reported that ROS significantly increased mitochondrial oxidative stress in yak meat, as evidenced by decreased activity of antioxidant enzymes and increased lipid peroxidation, and affected the tenderness during postmortem aging by activating the mitochondrial apoptotic cascade reaction (Wang et al., 2018).

Ferroptosis is a new iron-dependent form of programmed cell death induced by the metabolism of iron, lipid peroxidation, amino acid and ROS, which is morphologically characterized by a reduction or disappearance of the mitochondrial cristae, rupture of the mitochondrial outer membrane and an increase in the density of the mitochondrial membrane (Li et al., 2022). Mitochondria as regulators of cell metabolism, signal transduction and cell death, have been shown to generate and mediate ferroptotic signaling as they contain majority of components of ferroptotic machinery. Meanwhile, ferroptotic signaling molecules are involved in other types of cell death that may interact and occur simultaneously under pathological conditions (Javadov, 2022). Therefore, mitochondrial oxidative stress may be an important pathway for inducing ferroptosis and may affect the tenderization of postmortem muscle tissue. However, to our knowledge, little has been known about how ferroptosis affects meat quality and the role of mitochondria, Chen et al. (2022) found that oxidative stress induced by H_2O_2 exposure resulted in mitochondrial damage, iron overload and ferroptosis pathway activation, leading to the deterioration of broiler meat quality. Zhang et al. (2022)

evaluated the effects of bile acids' supplementation on fat deposition in lambs, and found that ferroptosis and fatty acid biosynthesis may be the major pathway regulating fat deposition, resulting in the production of higher quality lamb meat with less fat. Our previous studies identified ferroptosis in beef tissues during refrigeration and elucidated the molecular mechanism of ferroptosis based on the mediation of ferritin, heme, etc. and its effect on water holding capacity (Liu et al., 2022, 2023a, 2024). However, the possible mechanisms by which mitochondria are involved in ferroptosis in refrigerated beef have not been investigated, and whether mitochondrial oxidative stress-mediated ferroptosis affects beef tenderness during refrigeration remains unknown.

Given the complexity of relationships between mitochondria and ferroptosis, there is an urgent need to investigate the underlying mechanisms to reveal the effects on beef tenderness. In this study, morphological, physiological and biochemical indicators were used to determine the extent of mitochondrial damage, mitochondrial antioxidant capacities and mitochondrial free iron, so as to evaluate the level of mitochondrial oxidative stress and ferroptosis in refrigerated beef. The quantitative proteomics based on full tandem mass tag (TMT) of mitochondrial was further used to characterize the expression levels and pathways enrichment of the relevant proteins, and clarify the mechanism of mitochondrial oxidative stress-mediated ferroptosis. In addition, the relationship between ferroptosis and tenderness of refrigerated beef was also analysed. The results of this study expand the knowledge of mitochondrial regulation of ferroptosis in refrigerated beef, and may provide a theoretical basis for the regulation and control of tenderness in postmortem beef.

2. Materials and methods

2.1 Materials

Eight simmental cattle (bulls, 18-24 months old, body weight 400 ± 25 kg) with the same diet were slaughtered by a commercial method at Ningxia Yitai Herding Co. according to the guidelines of the Canadian Council on Animal Care. The longissimus dorsi (LD) muscle were collected in a ziplock bags, placed in a styrofoam box containing ice packs and sent to the laboratory within 2 h. The muscle samples were cut into pieces (average weight 150 ± 2.5 g) and any visible external fat and connective tissues were trimmed. A total of 40 pieces of muscles were randomly assigned into five groups (n = 8) and then placed onto PP plastic trays (length, 180 mm; height, 20 mm; width, 115 mm) covered with PVC plastic wrap. Samples were stored and collected at 0, 1, 3, 5 and 7 days (4.0 ± 0.5℃) and immediately divided into two batches: one batch was collected for biochemical analysis, and the other was frozen in liquid nitrogen and stored at −80℃ for later determinations.

2.2 Shear force value and texture profile

The shear force value and texture profile analyses (TPA) were determined according to Park et al. (2019). The meat blocks (2.5 cm in diameter) were put into plastic bags and heated in a water bath at an internal temperature of 75℃ for 10 min, samples were then taken out and cooled down to room temperature. Cooked samples were cut into small pieces (2 cm×1 cm×1 cm) with a scalpel for shear force determination, sheared perpendicularly to the muscle fibers at a shearing speed of 60 mm/min using a texture analyzer (TMS-Pro, Food Technology Corporation—FTC Co.,

West Sussex, VA, USA) equipped with 250 N load cell and a shear probe. The determinations were conducted six times. Besides, the texture profile (including cohesiveness, springiness, chewiness and hardness) was determined using the texture analyzer equipped with 1000 N load cell and a cylindrical probe (7.5 cm in diameter), and the samples (1.5 cm×2 cm×1.5 cm) were compressed twice to 30% of their initial height at a speed of 60 mm/min.

2.3 Myofibrillar fragmentation index (MFI)

MFI was measured based on a previous report (Huang et al., 2023). Briefly, 1 g of meat was homogenized using a homogenizer (HM7300, Laipu Ltd., Beijing, China) with 10 mL precooled buffer (4℃, 0.1 mol/L KCl, 20 mmol/L K_2HPO_4, 1 mmol/L Na_2EDTA and 1 mmol/L $MgCl_2$, pH 7.1) for 30 s every 1 min twice. Samples were then centrifuged at 4500 r/min, 4℃ for 15 min, and the supernatant was discarded while the pellet was re-suspended in 10 mL of the buffer for protein concentration determination by BCA Assay Kit (Nanjing Jiancheng Bioengineering Institute, Nanjing, China). The absorbance was determined at 540 nm using an UV-spectrophotometer (UV-9000S Metash Instruments Co. Ltd, Shanghai, China) following the adjustment to 0.5 mg/mL. Finally, the absorbance was multiplied by 200 as MFI.

2.4 Transmission electron microscopy (TEM)

The trimmed meat samples (0.5 cm×0.5 cm×0.5 cm) were placed in tenfold the volume of 2.5% glutaraldehyde, pre-fixed at 4℃ for 12 h and washed with phosphate buffer (0.28 M NaH_2PO_4, 0.72 M Na_2HPO_4, pH 7.2) for 4 times (10 min/time). Then, the tissues were fixed in 1% osmium tetroxide for 30 min and dehydrated through an

ethanol series (30%, 50%, 70%, 80%, 90%, 95%), and finally in 100% ethanol for 3 times (10 min/time). The tissues were embedded in epoxy resin embedding media and sliced with an ultramicrotome (Leica UC7rt, Wetzlar, Germany), thin sections were stained with uranyl acetate followed by lead citrate, the myofibrillar microstructure and ultrastructure of intermyofibrillar mitochondria were then observed using a TEM (JEM-1400Flash, JEOL Ltd., Tokyo, Japan) (Yu et al., 2020).

2.5 Mitochondrial extraction

Mitochondria were isolated by differential centrifugation (Ke et al., 2017; Zou et al., 2022). Briefly, 10 g of meat were washed twice with 250 mM sucrose, and then, homogenized with 20 mL mitochondrial isolation buffer (250 mM sucrose, 10 mM Tris-HCl, 1 mM EDTA, 0.1% BSA, pH 7.2), trypsin (≥250 N.F.U/mg) was subsequently added and incubated for 20 min. The hydrolyzed sample was diluted to 100 mL using mitochondrial isolation buffer and homogenized again, and the homogenate was then centrifuged at 1500 g, 4℃ for 15 min to collect the supernatant, which was then centrifuged at 12000 g, 4℃ for 20 min. The precipitated mitochondria were obtained and resuspended using mitochondrial suspension (250 mM sucrose, 10 mmol/L Tris-HCl, pH 7.4) after two washes in mitochondrial isolation buffer. Mitochondrial protein content was quantified by the BCA method for further analyses.

2.6 Mitochondrial swelling

Briefly, 3 mL of mitochondria (0.5 mg/mL protein) were mixed with 0.4 mL of $FeSO_4$ (0.5 mM) and 0.4 mL vitamin C (0.5 mM), and incubated at 37℃ for 15 min. Then, an absorbance measurement was conducted at 520 nm. The lower absorbance indicates a

greater degree of mitochondrial swelling (Zhang et al., 2018).

2.7 Measurement of mitochondrial ROS level

ROS level was measured according to a previous report (Wang et al., 2018). Mitochondria (0.1 mg/mL of protein) was uniformly mixed with precooled phosphate buffer (50 mmol/L, 5 μM DCFH-DA, pH 7.4). The mixture was incubated in a water bath at 37 °C in the dark for 15 min, and centrifuged at 12000 g, 4 °C for 15 min. Then, the fluorescent intensity was recorded at 488 nm excitation and 525 nm emission wavelength by a fluorescence spectrophotometer (970CRT Shanghai Precision & Scientific Instrument Co. Ltd, Shanghai, China).

2.8 Measurement of mitochondrial permeability transition pore (MPTP) opening

The protein concentration of mitochondria was adjusted to 0.3 mg/mL by the MPTP buffer (230 mmol/L mannitol, 70 mmol/L sucrose, 3.0 mmol/L Hepes, pH 7.4). Then 1 mL of mitochondrial suspension was mixed with 3 mL of MPTP test medium, and absorbance was determined at 540 nm using an UV-spectrophotometer (UV-9000S Metash Instruments Co. Ltd, Shanghai, China) (Li et al., 2023).

2.9 Mitochondrial free iron determination

The content of mitochondrial free iron was determined using a method as described previously (Liu et al., 2023b) with modifications. Briefly, mitochondrial sample was suspended in 8 mL ultrapure water, sonicated for 20 min, and centrifuged at 16000 g for 10 min. Then, the supernatant was centrifuged at 5000 r/min for 50 min using the Amicon Ultra-15 ultrafiltration centrifugal filter (3000 MW cutoffs), about 4 mL of filtrate were used for the ICP-MS analysis (Agilent 7800, Agilent Technologies Inc.,

198 USA). The standard curve was y = 1152.0545x + 7024.5459, R^2 = 0.9997. The iron
199 content was expressed as μg/g protein.

200 **2.10 Determination of mitochondrial antioxidant capacities**

201 The levels of reduced glutathione (GSH), malondialdehyde (MDA), total
202 antioxidant capacity (T-AOC) and activities of glutathione peroxidase (GPX) were
203 analysed by using Assay Kits (Jiancheng Bioengineering Institute, Nanjing, China).

204 **2.11 Mitochondrial proteomics**

205 **2.11.1 Sample preparation and digestion**

206 Mitochondrial proteins were extracted using a mitochondrial extraction kit (Solarbio,
207 Beijing, China) in accordance with the kit instructions. Briefly, mitochondria were
208 extracted using differential centrifugation at 4°C throughout the process, and washed
209 several times to remove impurities, ensuring that mitochondrial proteins with high
210 purity were obtained. Then, 400 μL of SDT-lysis buffer (4% SDS, 100 mM DTT, 150
211 mM Tris-HCl, pH 8.0) were added, heated in water bath at 95°C for 3 min, sonicated
212 for 2 min, and centrifuged at 16000 g, 4°C for 20 min. The supernatants were taken out
213 and quantified using the BCA method. Dithiothreitol (DTT, 100 mM) was added to each
214 sample, and the mixture was cooled down to room temperature after 5 min in a boiling
215 water bath. Then, UA buffer (8 M urea, 150 mM Tris-HCl, pH 8.0) was added and
216 centrifuged at 12000 g for 15 min by repeated ultrafiltration (Microcon units, 10 kD),
217 the filtrate was discarded and 100 μL iodoacetamide (IAA) (50 mM IAA in UA buffer)
218 was added and incubated at room temperature for 30 min in the dark after being shaken
219 at 600 rpm for 1 min, and centrifugated at 12000 g for 10 min. Then, 100 μL of UA

buffer was added, centrifuged at 12000 g for 10 min, and repeated the steps twice. After 100 μL NH_4HCO_3 buffer was added, samples were centrifuged at 14000 g for 10 min, and the steps repeated twice. The precipitates were collected and dissolved in 60 μL trypsin buffer (6 μg trypsin in 40 μL NH_4HCO_3 buffer), shaken at 600 rpm for 1 min, and digested at 37°C for 16 h. Finally, the resulting filtrate was collected via centrifugation (12000 g, 10 min), and the peptides were desalted using a desalting spin column (Thermo Fisher Scientific, Waltham, MA, USA) for quantification.

2.11.2 TMT labelling

Briefly, 100 μg of the peptides were taken from each sample and labeled according to TMT labeling kit instructions (Thermo Fisher Scientific, Waltham, MA, USA). Samples were mixed with an equal number of peptides from the same groups. Each aliquot (100 μg of peptide equivalent) was reacted with one tube of TMT reagent. Then, the sample was dissolved in 100 μL of TEAB solution (0.05 M, pH 8.5), and the TMT reagent was dissolved in 41 μL of anhydrous acetonitrile. The mixture was incubated at room temperature for 1 h. Then, 8 μL of 5% hydroxylamine were added to the sample and incubated for 15 min to quench the reaction. The multiplex labeled samples were pooled together and lyophilized. And then, samples were mixed and fractionated by using pierce high-pH reversed-phase peptide fractionation kit (Thermo Fisher Scientific) to increase the number of peptide identifications. Finally, the peptides of each fraction were dissolved in 0.1% formic acid for LC-MS analysis.

2.11.3 LC-MS/MS analysis

LC-MS analysis was performed on a Q Exactive mass spectrometer coupled to Easy

nLC (Thermo Fisher Scientific, Waltham, MA, USA). Peptide from each fraction was loaded onto a C_{18}-reversed phase column (12 cm long, 75 μm ID, 3 μm) in buffer A (2% acetonitrile and 0.1% formic acid) and separated with a linear gradient of buffer B (90% acetonitrile and 0.1% formic acid) at a flow rate of 300 nL/min over 60 min. The linear gradient was set as follows: 0–2 min, linear gradient from 2% to 5% buffer B; 2–42 min, linear gradient from 5% to 20% buffer B; 42–50 min, linear gradient from 20% to 35% buffer B; 50–52 min, linear gradient from 35% to 90% buffer B; 52–60 min, buffer B maintained at 90%. The MS data were obtained with a data-dependent mode selecting dynamically the precursor ions from the survey scan (300–1800 m/z) for the higher energy collisional dissociation (HCD) fragmentation. Determination of the target value was based on predictive automatic gain control (pAGC). The automatic gain control (AGC) target values were set at 1e6, with maximum injection time of 50 ms for full MS, and a target AGC value was set at 1e5, with maximum injection time of 100 ms for MS2. Dynamic exclusion duration was 30 s. Survey scans were acquired at a resolution of 70000 at 200 m/z and resolution for HCD spectra was set to 35000 at 200 m/z. Normalized collision energy was 30. The instrument was run with peptide recognition mode enabled.

2.11.4 Database searching and analysis

The resulting LC-MS/MS raw files were imported into MaxQuant software (version 1.6.0.16, Thermo Fisher Scientific, Waltham, MA, USA) for data interpretation and protein identification against the database Uniprot_Hordeum-vulgare_201747-20180125 (downloaded on 25/01/2018, and including 201747 protein sequences),

which was sourced from the protein database at https://www.uniprot.org/uniprot/?query=Hordeum-vulgare&sort=score. An initial search was set at a precursor mass window of 6 ppm. The search followed an enzymatic cleavage rule of Trypsin/P and allowed maximal two missed cleavage sites and a mass tolerance of 20 ppm for fragment ions. The modification set was as following: fixed modification: Carbamidomethyl (C), TMT10plex(K), TMT10plex(N-term), variable modification：Oxidation(M) and Acetyl (Protein N-term). The minimum 6 amino acids were required for peptide, and ≥1 unique peptides were required per protein. For peptide and protein identification, false discovery rate (FDR) was set at 1%. TMT reporter ion intensity was used for quantification.

2.11.5 Bioinformatics analysis

Bioinformatics analyses were carried out with Perseus software (Max-PlanckInstitute of Biochemistry—Computational, Systems, Biochemistry), Microsoft Excel (Microsoft Office 2019, Redmond, DC, USA) and R statistical computing software (R Foundation for Statistical Computing, Vienna, Austria). Differentially expressed proteins (DEPs) were screened with the cutoff of a ratio fold-change of >1.20 or <0.83 and *p*-values <0.05. Expression data were grouped together by hierarchical clustering according to the protein level. To annotate the sequences, information was extracted from UniProtKB/Swiss-Prot (https://www.expasy.org/resources/uniprotkbswiss-prot), Kyoto Encyclopedia of Genes and Genomes (KEGG) (http://geneontology.org/), and Gene Ontology (GO) (http://www.geneology.org/). GO and KEGG enrichment analyses were carried out

with the Fisher's exact test, and FDR correction for multiple testing was also performed. The protein-protein interaction (PPI) analysis of 7 DEPs enriched into the ferroptosis pathway was performed by STRING software version 12.0 (http://string-db.org/).

2.12 Parallel reaction monitoring (PRM) validation

To verify the protein expression levels obtained by TMT quantitative proteomics analysis, DEPs with reliable identification information were selected for further targeted quantified by LC-PRM/MS. In brief, peptides were prepared according to the TMT proteomics, PRM analysis was performed on a Exactive HF-X mass spectrometer (Thermo Fisher Scientific, Waltham, MA, USA), which was operated in positive ion mode (300-1200m/z) and with the following parameters: the resolution of first-order mass spectrometry: 70000 (200 m/z), AGC target: 3e6, maximum IT: 50 ms; the resolution of second-order mass spectrometry: 30000 (200 m/z), AGC target: 1e6, maximum IT: 100 ms, activation type: HCD，isolation window: 1.6 Th, normalized collision energy: 28. The raw data were analyzed using Skyline (MacCoss Lab, University of Washington, USA).

2.13 Statistical analysis

All experiments were conducted in triplicate. Results were expressed as mean ± standard deviation (SD). Data were analyzed by ANOVA, followed by Duncan's test to analyze the significance (p<0.05) by SPSS software v19.0 (SPSS, Inc., Chicago, IL, USA). Multivariate statistical analysis and graphical work were performed by OriginPro software v2023 (OriginLab, Northampton, MA, USA), graphical abstract was created using biorender.com.

3. Results and discussion

3.1 Beef tenderness

Shear force is a commonly used indicator for evaluating meat tenderness, meat tenderness can be inversely represented by shear force, the lower shear force usually results in more tender meat. As shown in Fig. 1a, the shear force of beef first increased and then decreased sharply, and the maximum shear force value (115.52 ± 3.96 N) on day 3 was significantly higher than those of other groups (p<0.05), indicating day 3 could be the postmortem rigor mortis stage of beef muscle (Wang et al., 2018). However, the shear force decreased continuously from 5 to 7 d, and 7 d was significantly lower than the others (p<0.05), indicating the best tenderness. The improvement of muscle tenderness at later aging stage has become a consensus, and the tenderness of postmortem muscle is a complex quality attribute, which is the result of multiple interwoven factors. Chen et al. (2022) reported that the high glycolysis rate induced by ROS accumulation accelerated the postmortem tender process, leading to a lower final shear force value. In addition, accumulation of hydrogen ions produced by glycolysis reduced pH in post-mortem muscle, which drove Ca^{2+} overload and activated a series of Ca^{2+}-dependent proteases, accelerating cell death and improving beef tenderness (Xin et al., 2023). Moreover, cathepsin B and L were found to degrad myofibrillar proteins and collagen, and its activity has been shown to increase significantly with aging time, thus contributing to the tenderization of postmortem beef (Wang et al., 2022). MFI is notable for measuring both I-band breaks and myofibril integrity loss in order to estimate meat tenderness and proteolysis, which has been shown to explain

more than 50% of the variation in tenderness (Smili et al., 2022; Xin et al., 2023). MFI in all samples significantly increased (p<0.05) (Fig. 1b), indicating the sustained breakdown of myofibril. Similarly, Chen et al. (2020) found that MFI increased significantly over the whole aging process in beef, suggesting that beef tenderization persisted after slaughter. Interestingly, beef shear force did not decrease with the increase of MFI at the early refrigeration stage. A similar result was reported by Bai et al. (2023). This may be due to the fact that MFI was not the dominant factor effecting beef shear force at the early aging stage.

The myofibrillar microstructure of beef samples was further analyzed to explain the changes in tenderness. As shown in Fig. 1c, the sarcomere structure was neatly arranged and well defined at 0 d, and Z−disk and M−disk were clearly visible as well. As the storage period progressed, slight rupture began to occur at the junction of the adjacent sarcomeres, accompanied by the gradual expansion of myofibrillar gaps from 1 to 3 d. However, at this point, the Z−disk and M−disk were still visible and the I−band and A−band could be clearly distinguished. Recent study reported that the breakdown, deformation and gap enlargement of myofibrils may create the channel for water loss and reduce the water-holding capacity (WHC) of the beef meat (Liu et al., 2023b), and the contraction of muscle fibers at the early postmortem stages also compressed the water storage space, resulting in water loss (Lei et al., 2022), and it was noteworthy that the decrease in WHC had a negative effect on the tenderization of meat. In the later stages of storage (from 5 to 7 d), extensive degradation of myofibrils was observed, the Z−disk and M−disk were almost completely disintegrated, and the I−band and A−band

352 became unrecognizable in 7 d, resulting in a sparser tissue structure, which was one of
353 the reasons for the rapid decline in beef tenderness at the later stage of storage. Z−disk
354 served as a connection between adjacent sarcomere, and the destruction of the Z−disk
355 structure led to the disintegration and fragmentation of myofibril (Li et al., 2022).
356 Obviously, the microstructural observations of myofibrillar were highly consistent with
357 MFI results.

358 Hardness, chewiness, cohesiveness and springiness were the important characteristic
359 parameters to evaluate the effectiveness of meat processing, packaging and storage (Li
360 et al., 2022). As shown in Table 1, the hardness tended to increase first and then decrease
361 throughout the entire refrigeration period, with the maximum at 3 d (60.27 N), which
362 corresponded well to the shear force result. The decline in meat hardness was reported
363 to be related to tenderization caused by protein degradation (Zhang et al., 2023).
364 Chewiness has a positive correlation with hardness, cohesiveness and springiness. In
365 this study, chewiness showed the same trend as hardness, dropping sharply on 5 d of
366 storage. Meanwhile, it was found that hardness and chewiness showed greater values
367 and variations than other texture indicators, consistent with the texture results in cooked
368 meat products and contributed more to the formation of the final texture of the meat
369 (Supatcharee et al., 2023). Moreover, the cohesiveness and springiness fluctuated both
370 up and down during the refrigerated storage period, which were influenced by the
371 formation of protein-protein interactions and changes in protein gel properties in meat
372 (Zhang et al., 2021). However, during the aging and storage process of post−slaughter
373 muscle, myofibrillar degradation, water loss, internal and external enzyme release were

still the main physiological and biochemical changes, which caused the dominant position of hardness and chewiness in the texture analysis of meat (Lei et al., 2022; Zhang et al., 2019). These observations further demonstrated the intrinsic reasons for the changes in beef tenderness during refrigerated storage.

3.2 The extent of mitochondrial damage

Numerous studies confirmed that the mitochondrial pathway is the main producer of ROS in cells and tissues, including oxygen radicals and nonradical derivatives of oxygen such as hydroxyl free radical, singlet oxygen, nitric oxide and hydrogen peroxide (Xie et al., 2023; Yu et al., 2020). Meanwhile, the production of ROS is a positive feedback mechanism, which will increase the permeability of mitochondrial pores, thus leading to mitochondrial dysfunction and further production of ROS (Bergandi et al., 2022). As shown in Fig. 2a, mitochondrial ROS level increased in the first 3 days and reached a maximum at 3 d, with a decline at 5 d. After slaughter, muscle is in a pathophysiological state of energy and oxygen deficiency, leading to redox imbalance and oxidative stress, accompanied by the dynamic equilibrium of intracellular ROS production and scavenging disrupted, ultimately, excess ROS is produced, resulting mitochondrial dysfunction with damage to the mitochondrial membrane (Li et al., 2023; Chen et al., 2020). Thus, it was speculated that a large amount of ROS may be generated due to an imbalance of the mitochondrial redox system in the first 3 days of storage, with the attack of ROS on the mitochondrial structure, the mitochondrial structure is damaged and the function is lost, ROS production cannot continue and spread to the cytoplasm, therefore, the mitochondrial

ROS content gradually decreased in the later stage of beef storage. In addition, it was found that ROS-induced oxidative stress significantly increased the MPTP (Gamage et al., 2022; Chen et al., 2020). MPTP was inversely proportional to the absorbance, as shown in Fig. 2b, the continuous decrease in absorbance indicated that MPTP increased with the extension of storage period. In particular, the significant decrease (p<0.05) in the first three days confirmed the high production of ROS in the early stage of storage, and the increased mitochondrial membrane permeabilization led to the release of mitochondria proteins and cell death (Sebag et al., 2018).

Moreover, mitochondrial swelling measurements showed a similar conclusion (Fig. 2c), the lower the absorbance value, the more serious the mitochondrial swelling. In combination with the ultrastructure of intermyofibrillar mitochondria (Fig. 2d), the mitochondrial structure of 0 d samples was relatively complete, with a compact cristae structure and clear fold arrangement, mitochondrial swelling, vacuolization and cristae decrease occured at 1 d, and further aggravated from 3 to 5 d samples, at 7 d of storage, the mitochondrial membrane was severely ruptured, and only vague partial ridge fragments were observed. These observations in mitochondrial ultrastructure were similar to the morphological features of ferroptosis. Ferroptosis has unique morphological features distinct from apoptosis, necrosis and autophagy, excluding features such as apoptotic body formation, rupture of cell membrane and autophagosome formation, which are predominantly embodied in mitochondria, including mitochondrial outer membrane rupture, mitochondrial cristae reduction and condensed mitochondrial membrane density (Zhang et al., 2022; Sun et al., 2023). To

418 further verify the level of ferroptosis during beef refrigeration, the free iron content in
419 mitochondria was determined. Previous studies reported that mitochondria were an
420 important locus for ferroptosis, as they were rich in lipids and iron (Battaglia et al.,
421 2020; Xue et al., 2022), and mitochondrial iron was primarily utilized for biosynthesis
422 of heme iron and iron–sulfur clusters. As shown in Fig. 2e, the content of mitochondrial
423 free iron increased significantly with storage time (p<0.05). The disturbed iron
424 homeostasis and abnormal iron accumulation was the signs of ferroptosis (Tang et al.,
425 2022), iron participates in the accumulation of mitochondrial ROS, excessive iron
426 produces a large number of mitochondrial ROS and hydroxyl radicals through Fenton
427 reaction to attack mitochondrial membrane, resulting in lipid peroxidation, damage to
428 membrane integrity and protein function, and eventually leading to ferroptosis
429 (Battaglia et al., 2020).

430 Therefore, it was concluded that the ferroptosis characteristics appeared in
431 mitochondria during the beef refrigeration, and it was speculated that oxidative stress
432 of mitochondria may induce ferroptosis, but further confirmation is needed.

433 **3.3 Mitochondrial antioxidant capacities**

434 In addition to abnormal iron metabolism, accumulation of ROS and mitochondrial
435 morphological characteristics, ferroptosis is also characterized by glutathione
436 metabolism disorders, lipid peroxidation and so on (Zhang et al., 2023). To further
437 confirm the reliability of ferroptosis induced by mitochondrial oxidative stress,
438 antioxidant capacity of mitochondria was measured. In skeletal muscle, glutathione
439 metabolism is critical to the protection against oxidative stress, the core of ferroptosis

is the breakdown of the GSH−GPX4 antioxidant system, which cannot clear toxic lipid peroxidation (LPO) caused by Fe^{2+}, thus damaging cells (Zhou et al., 2022). As an essential cofactor of GPX, GSH can maintain redox state in mitochondria under normal physiological conditions, as shown in Fig.3 (a−b), the GSH content and GPX activity of mitochondria showed the same downward trend during refrigeration, which may be due to the inhibition of the cystine/glutamate antiporter responsible for cysteine import, leading to GSH depletion, low GPX activity and ferroptosis (Javadov, 2022). T−AOC reflects the overall antioxidant defense level of the organism. The decline of T−AOC (Fig. 3c) confirmed an imbalance in the mitochondrial redox system, the T-AOC at 3 d, 5 d and 7 d decreased significantly ($p<0.05$) (by 23.93%, 57.19% and 67.49% respectively, compared with 0 d), indicating the damage of the antioxidant defense system. In addition, mitochondrial membrane lipids contain abundant polyunsaturated fatty acid (PUFA), MDA is a by-product of PUFA robbed of hydrogen atoms by ROS and further decomposed by oxidation, and is used as an indicator of LPO (Liu et al., 2023b). The high level of MDA content at 3-7 d (Fig. 3d) indicated strong oxidative damage to mitochondria during the middle and late stages of refrigeration.

In conclusion, mitochondria are the major source and target of ROS, and contain main components of ferroptosis. In our study, ferroptotic features were observed in the mitochondria of beef during refrigeration, including mitochondrial iron accumulation, glutathione redox imbalance, impaired antioxidant defense system, lipid peroxide accumulation and morphological damage of mitochondria. Mitochondrial iron overload increased oxidative stress by generating ROS via Fenton reaction, and involved cellular

462 metabolism leading to the ferroptotic cell death.

463 **3.4 LC-MS/MS analysis**

464 **3.4.1 Quality control and data quality of samples**

465 As shown in Fig. 4a, the distribution patterns of different molecular weight bands of
466 proteins in different groups were similar and uniform, indicating that the protein
467 extraction effect was stable. Boxplot showed the median and quartiles of the samples,
468 the median of the samples in the same group was close to the same horizontal line (Fig.
469 4b), indicating good data quality and repeatability. In addition, Pearson correlation
470 coefficient was used to assess the correlation between samples, and the correlation
471 coefficient was greater than 0.982 (Fig. 4c), indicating small individual differences and
472 high data reproducibility.

473 **3.4.2 Differentially expressed proteins (DEPs) analysis**

474 A total of 2655 proteins were identified and quantified by TMT labeling quantitative
475 proteomics (Table S1), and 429 proteins showed significant expression differences (p
476 <0.05) (Table S2). Fig. 5a described the hierarchical clustering analysis heatmap of
477 the DEPs in beef mitochondria at different refrigeration stages, the expression
478 distribution of DEPs varied significantly in different mitochondrial samples. However,
479 hierarchical clustering analysis revealed a certain regularity in the expression pattern of
480 DEPs, and the samples were clustered into three groups (0d, 1 d and 3 d, 5 d and 7 d),
481 indicating that the mitochondrial samples from 1 d and 3 d, and from 5 d and 7 d had
482 similar DEPs, which could be distinguished from the samples from 0 d. This further
483 suggested that beef mitochondria underwent phasic changes with prolonged

refrigeration periods. Additionally, the DEPs at 1 d, 3 d, 5 d and 7 d samples were analyzed using 0 d as the control group, the volcano plots and bar graph (Fig. 5b-f) showed that 114, 192, 188 and 439 DEPs ($p<0.05$ and fold change>1.2, fold change <0.86), respectively, with 36, 69, 40 and 164 up-regulated, and 78, 123, 148, and 275 down-regulated respectively. Increases in the overall number of DEPs indicated intensified changes in mitochondrial structure and function. Besides, Venn plot was used to compare the overlap of differentially expressed patterns of DEPs assigned to each pairwise comparison. As shown in Fig.5g, four pairwise comparisons exhibited 48 overlapping DEPs, and 16, 57, 17 and 231 DEPs were only found in the 1 d vs 0d, 3 d vs 0 d, 5 d vs 0 d and 7 d vs 0 d comparisons, respectively, which may serve as potential biomarkers of the changes in beef mitochondria during refrigeration.

3.4.3 Functional analysis of DEPs

To obtain systematic insights into the functions of DEPs, the GO enrichment analysis and KEGG pathway analysis were further performed. DEPs were assigned into three major functional categories in GO analysis, namely biological process (BP), cellular component (CC) and molecular function (MF), top 10 enriched functions in the BP, CC and MF terms were shown in Fig. 6a. DEPs enriched in BP were mainly involved in positive regulation of cellular component movement (GO:0051272, n=10), response to endoplasmic reticulum stress (GO:0034976, n=13), positive regulation of locomotion (GO:0040017, n=9), positive regulation of cell motility (GO:2000147, n=9) and regulation of locomotion (GO:0040012, n=13). DEPs enriched in CC were mainly involved in endoplasmic reticulum subcompartment (GO:0098827, n=35), nuclear

outer membrane-endoplasmic reticulum membrane network (GO:0042175, n=35), endoplasmic reticulum membrane (GO:0005789, n=34), endoplasmic reticulum (GO:0005783, n=47) and organelle subcompartment (GO:0031984, n=35). DEPs enriched in MF were mainly involved in protein kinase activity (GO:0004672， n=6), protein serine/threonine/tyrosine kinase activity (GO:0004712, n=5), protein serine kinase activity (GO:0106310, n=5), phosphotransferase activity, alcohol group as acceptor (GO:0016773, n=7) and purine ribonucleoside triphosphate binding(GO:0035639, n=37). In addition, as shown in Fig. 6b, the top 30 predicted pathways by KEGG were mainly involved in phagosome (ID:bta04145, n=14), tight junction (ID:bta04530, n=14), regulation of actin cytoskeleton (ID: bta04810, n=16), ferroptosis (ID:bta04216, n=7), protein processing in endoplasmic reticulum (ID:bta04141, n=17), pathways of neurodegeneration-multiple diseases (ID:bta05022, n=34), parkinson disease (ID: bta05012, n=22), metabolic pathways (bta01100, n=63) and oxytocin signaling pathway (bta04921, n=11), suggesting that post-slaughter beef undergoes changes in protein backbone and lipid metabolism with mitochondria as the regulatory vehicle. Among them, the discovery of the ferroptosis pathway in beef mitochondrial proteomics demonstrated that mitochondria played an important role in ferroptotic cell death.

3.4.4 Ferroptosis pathway analysis

We further investigated DEPs enriched in the ferroptosis pathway to reveal the main molecular mechanism of ferroptosis in beef mitochondria during refrigeration. As shown in Fig. 7a, 7 DEPs were enriched to the ferroptosis pathway, including long-

chain-fatty-acid-coa ligase (ACSL) 1, ferritin (LOC788801), acyl-coa synthetase long chain family member (ACSL) 4, major prion protein (PRNP), voltage-dependent anion-selective channel protein (VDAC) 2, acyl-coa synthetase long chain family member (ACSL) 3 and lysophosphatidylcholine acyltransferase (LPCAT) 3, respectively. Subcellular localization analysis revealed that the identified ferroptosis DEPs mainly functioned in the membrane, cytoplasm, mitochondrion, endoplasmic reticulum and golgi apparatus (Fig. 7b). Previous studies have found that the main mitochondrial pathways involved in ferroptosis mainly include glutaminolysis, fatty acids metabolism, iron metabolism, redox status regulation, voltage-dependent anion channels regulation and citric acid cycle (TCA) (Battaglia et al., 2020; Javadov et al., 2022). In this study, it was found that the mitochondrial DEPs involved in ferroptosis during beef storage were concentrated in the lipid metabolism, iron metabolism and voltage-dependent anion channels regulation (Fig. S1).

Therein, ACSL1, ACSL3 and ACSL4 are the members of acyl-coa synthetase long chain (ACSL) family that insert into the outer mitochondrial membrane (OMM), endoplasmic reticulum membrane, and plasma membrane to participate in lipid metabolism pathway (Goetzman et al., 2020). Meanwhile, ACSL4 is involved in the arachidonic acid (AA) metabolism pathway as a key enzyme, representing the main process of lipid peroxidation (Shi et al., 2023). The expression of ACSL4 was firstly upregulated and subsequently downregulated, indicating that the mitochondrial lipid metabolism was disturbed and accompanied by increased lipid peroxidation in the pre-storage period (Fig. 3d), while the mitochondrial lipid peroxidation reaction was

reduced in the post-storage period, probably caused by the impaired mitochondrial structure and function. Mitochondria are highly susceptible to oxidative damage and lipid peroxide due to their lipid bilayer membranes and large crista surface area (Joubert and Puff, 2021). Moreover, mitochondrial lipid metabolism is an important source of lipid peroxide accumulation, which is the fatal event in the execution of ferroptosis (Guo et al., 2022). Therefore, in conjunction with our results, it is speculated that the lipid metabolism pathway may be the main mitochondrial pathway involved in ferroptotic cell death during beef refrigeration. Besides, PPI network analysis (Fig. 7c) showed that LPCAT3 and LOC788801 interacted with ACSLs involved in regulating ferroptosis. LPCAT3 can utilize lysophospholipids and AA-CoA produced by ACSL4 as substrates for phosphatidylation, and is considered to be an essential regulator of ferroptotic signaling (Bebber et al., 2021; Javadov, 2022). Our results showed that the expression of LPCAT3 was slightly downregulated throughout the refrigeration process (Fig. 7a), indicating that LPCAT3 in mitochondria may have no obvious role in promoting mitochondrial lipid peroxidation, thus leading to ferroptotic cell death during the refrigeration process of beef. In addition, disordered iron metabolism is one of the characters of ferroptosis, ferritin is an iron storage protein necessary for iron homeostasis, and mitochondria are the main organelle for iron regulation, which occurs primarily in the mitochondrial matrix. Labile iron (Fe^{2+}) can be transported across the inner mitochondrial membrane (IMM) by the mitochondrial iron importers, including membrane transporter mitoferrin 1 (Mfrn1) and mitoferrin 2 (Mfrn2) (Paradkar et al., 2009). Mitochondrial ferritin (FtMt) is mainly utilized for iron-sulfur cluster biogenesis,

572 FtMt storage, heme synthesis and chelation of labile iron (Chen et al., 2019), and it is
573 widely recognized that decreased FtMt expression promotes mitochondrial free iron
574 accumulation, resulting in excessive mitochondrial ROS generation and ferroptosis
575 (Giuliani et al., 2022). However, mitochondrial proteomics results showed that ferritin
576 (LOC788801) was up-regulated during the refrigeration process, indicating an
577 excessive iron accumulation in mitochondria and activate regulation of mitochondrial
578 iron homeostasis, consistent with the observation of free iron accumulation in
579 mitochondria (Fig. 2e).

580 In addition, VDAC2 and PRNP were found to be DEPs enriched in the ferroptosis
581 pathway. VDACs are the most abundantly expressed protein family in OMM and
582 participate in the transmembrane transport of ions and metabolites (van der Reest et al.,
583 2018). Mitochondrial hyperpolarization after VDACs opening leads to mitochondrial
584 ROS formation, increased mitochondrial membrane potential, mitochondrial
585 dysfunction and cell death (DeHart et al., 2018). Downregulation of VDACs appears to
586 be a result of mitochondrial response to oxidative stress. Yagoda et al. (2007) found that
587 erastin treatment resulted in the production of lethal oxidizing substance by the cells,
588 which induced a self-regulatory response to down-regulate VDAC2. Van der Reest et
589 al. (2018) reported that mitochondrial VDAC2 and VDAC3 were oxidized to maintain
590 mitochondrial function in response to ROS generated by oxidative stress. Meanwhile,
591 it was found that VDAC2 negatively regulated Bak-dependent apoptosis and deletion
592 of VADC2, leading to apoptosis (Kontchou et al., 2022). Our results showed that
593 VDAC2 was down-regulated during refrigeration (Fig. 7a), probably due to oxidative

stress in the mitochondria of post-slaughter beef, which exhibited physiologically regulated reduction in VDAC2 expression and accelerated cell death including ferroptosis to some extent. PRNP participated in metal transportation and its expression was associated with the disruption of Fe and Cu metabolism imbalances (Rivera et al., 2015). PRNP was distinct from the transferrin bound iron-transferrin receptor 1 transport system, and had a unique iron ion transport mechanism that can transport Fe^{3+} into the cell via zinc transporters (ZIP8/ZIP14) on the cell membrane, converting it to Fe^{2+} (Liu et al., 2024). In this study, the expression of PRNP fluctuated depending on the refrigeration time, while the expression of PRNP was down-regulated compared to 0 d, indicating that PRNP may respond to the imbalance of iron ion metabolism. Other studies have also found that PRNP played a role in biological metabolism and disease induced by ferroptosis. For example, Zhou et al. (2021) found that PRNP was involved in adipocyte differentiation, suggesting that the ferroptosis pathway may be a key pathway for intramuscular fat deposition. Hong et al. (2021) reported that PRNP played a key role in colorectal cancer ferroptosis.

In summary, mitochondria play an important role in ferroptosis, and the mitochondrial pathways involved in ferroptosis are mainly fatty acids metabolism, iron metabolism and voltage-dependent anion channels regulation, which are complex and interact with each other in their mechanisms and work together in ferroptosis. The discovery of mitochondria-mediated ferroptosis and its mechanism during the post-slaughter refrigeration storage of beef supplemented the theoretical system of mitochondrial regulation of post-slaughter muscle physiology and biochemistry, and

provided theoretical guidance for the subsequent studies of ferroptosis-mediated beef quality.

3.4.5 Validation by PRM

Based on the results of TMT quantitative proteomic analysis, 10 proteins enriched in the ferroptosis pathway and fatty acid metabolism pathway with high abundance of plausible peptides were selected for validation by PRM analysis, including VDAC2, ACSL1, LPCAT3, VDAC3, TF, TFRC, PCBP1, CP, PCBP2 and ACADM (Table 2). The trends in the relative abundance of the 10 proteins during beef storage were in accordance with the results of TMT quantitative protein analysis (Table S1), indicating that the TMT quantitative protein analysis method was reliable.

3.5 Correlation between mitochondrial oxidative stress-mediated beef ferroptosis and tenderness

To further assess the potential effects of mitochondrial oxidative stress-mediated beef ferroptosis on beef tenderness, Spearman's correlation analysis was performed. As shown in Fig. 8, shear force was positively correlated with mitochondrial ROS ($p<0.05$), indicating that the process of beef muscle rigidity after slaughter was accompanied by mitochondrial ROS production and oxidative stress. MFI was significantly positively correlated with MPTP, mitochondrial swelling, the contents of mitochondrial free iron and MDA ($p<0.05$), while negatively significantly correlated with GSH, GPX, T-AOC, ACSL1, VDAC2, ACSL3, LPCAT3 ($p<0.05$). Notably, ACSL4 was significantly positively correlated with texture indicators (springiness, chewiness and hardness) ($p<0.05$), and the content of mitochondrial free iron was significantly positively

correlated with MDA, MFI, MPTP and mitochondrial swelling (p<0.05). These results suggested that oxidative stress was associated with abnormal mitochondrial iron metabolism after beef slaughter, resulting in mitochondrial ferroptosis characteristics, and iron overload may exacerbate oxidative attack on myofibrils and plasma membranes by generating excess ROS via the Fenton reaction, thus increasing MFI and aggravating lipid peroxidation. It has been reported that ROS could promote myofibrillar protein degradation, destroy the structure of muscle cells and ultimately affect muscle tenderness by accelerating muscle glycolysis and increasing caspases activities (Wang et al. 2018; Chen et al. 2022). Therefore, the activation of ferroptosis signaling pathway mediated by mitochondrial oxidative stress may have a positive effect on beef tenderization. In addition, mitochondrial structural changes may accelerate the release of tenderness-associated pro-cellular death factors, but further studies are needed to confirm this.

4. Conclusions

This study revealed the underlying mechanism of mitochondrial involvement in ferroptosis of refrigerated beef and its potential impact on tenderness formation. The results showed that mitochondrial oxidative stress-mediated ferroptosis was found in beef during refrigeration, which was manifested as glutathione redox imbalance, impaired T-AOC, mitochondrial free iron accumulation, MDA accumulation and morphological damage of mitochondria. Furthermore, seven DEPs enriched to the ferroptosis pathway were identified by mitochondrial TMT proteomics, including ACSL1, LOC788801, ACSL4, PRNP, VDAC2, ACSL3 and LPCAT3, which were

involved in lipid metabolism pathway, iron metabolism pathway and voltage-dependent anion channels regulation pathway, suggesting that mitochondria may be involved in ferroptotic cell death through regulation of free iron accumulation, lipid peroxidation and transmembrane transport, with the lipid metabolism pathway being the major mitochondrial pathway involved in ferroptosis during beef refrigeration. In addition, ferroptosis was dependent on iron and ROS accumulation, and iron-overload induced ROS production may attack tissue myofibrillar structure and exacerbate plasma membrane peroxidation, which participated and promoted the formation of postmortem meat tenderness. Overall, changes in postmortem muscle tenderness were influenced by multiple factors, which are interwoven rather than independent, and mitochondrial oxidative stress-mediated ferroptosis may be only one of the key pathways. Nevertheless, this finding expands the molecular theoretical system of how cell death affects tenderness of postmortem beef, which may provide new ideas for future research on physiology and biochemistry of postmortem meat and the regulation of meat tenderness.

CRediT authorship contribution statement

Ningxia Bu: Conceptualization, Methodology, Software, Writing—original draft. **Qi Yang:** Investigation, Formal analysis. **Weihua Liu:** Resources, Formal analysis. **Jun Liu:** Formal analysis, Visualization. **Anran Zheng:** Data curation, Visualization. **Yao Zhang:** Data curation, Validation. **Dunhua Liu:** Writing—review and editing, Funding acquisition.

Funding

This research was funded by the Ningxia Natural Science Foundation (2022AAC02021), Ningxia Key R & D plan (2021BEF02037), and Ningxia Science and Technology Innovation Team (2022BSB03108),

Declaration of Competing Interest

The authors declare that they have no known competing financial interests or personal relationships that could have appeared to influence the work reported in this paper.

Acknowledgment

The authors would like to thank Shanghai Bioprofile Co., Ltd. for providing technical support for TMT quantitative proteomics.

References

Adjei, V. Y., Mensah, G. I., Kunadu, A. P. H., Tano-Debrah, K., Ayi, I., & Addo, K. K. (2022). Microbial safety of beef along beef value chains in the ashaiman municipality of ghana. *Frontiers in Veterinary Science, 9*, 813422.

Arikawa, L. M., Mota, L. F. M., Schmidt, P. I., Frezarim, G. B., Fonseca, L. F. S., Magalhaes, A. F. B., Silva, D. A., Carvalheiro, R. Chardulo, L. A. L., & de Albuquerque, L. G. (2024). Genome-wide scans identify biological and metabolic pathways regulating carcass and meat quality traits in beef cattle. *Meat Science, 209*, 109402.

Bergandi, L., Apprato, G., & Silvagno, F. (2022). Antioxidant and anti-inflammatory activity of combined phycocyanin and palmitoylethanolamide in human lung and prostate epithelial cells. *Antioxidants, 11*(2), 201.

Battaglia, AM., Chirillo, R., Aversa, I., Sacco, A., Costanzo, F., & Biamonte, F. (2020).

Ferroptosis and cancer: Mitochondria meet the “Iron Maiden” cell death. *Cells, 9*(6), 1505.

Bebber, C. M., Thomas, E. S., Stroh, J., Chen, Z. Y., Androulidaki, A., Schmitt, A., Höhne, M. N., Stüker, L., Alves, C. D., Khonsari, A., Dammert, M. A., Parmaksiz, F., Tumbrink, H. L., Beleggia, F., Sos, M. L., Riemer, J., George, J., Brodesser, S., Thomas, R. K., Reinhardt, H. C., & von Karstedt, S. (2021). Ferroptosis response segregates small cell lung cancer (SCLC) neuroendocrine subtypes. *Nature communications, 12*(1), 2048.

Bai, X. Y., Yin, F., Ru, A., Tian, W., Chen, Q. W., Chai, R., Liu, Y. X., Cui, W. M., Li, J. H., Yin, M. C., Zhu, C. Z., Zhao, G. M. (2023). Effect of slaughter age and postmortem aging time on tenderness and water-holding capacity of yak (Bos grunniens) longissimus thoracis muscle. *Meat Science,* 202, 109201.

Chen C., Guo Z. B., Shi X. X., Guo Y. X., Ma G. Y., Ma J. B., & Yu Q. L. (2022). H_2O_2-induced oxidative stress improves meat tenderness by accelerating glycolysis via hypoxia-inducible factor-1α signaling pathway in postmortem bovine muscle. *Food Chemistry: X, 2022*(16), 100466.

Cheng C., Jiaying Z., Zhaobin G., Xixiong S., Yubin Z., Li Z., Qunli Y., & Ling H. (2020). Effect of oxidative stress on AIF-mediated apoptosis and bovine muscle tenderness during postmortem aging. *Journal of Food Science, 85*(1), 77-85.

Chen, C. L., Wang, S. C., & Liu, P. (2019). Deferoxamine enhanced mitochondrial iron accumulation and promoted cell migration in triple-negative MDA-MB-231 breast cancer cells via a ROS-dependent mechanism. *International Journal of Molecular Sciences, 20*(19), 4952.

726 Chen, Z. D., Xing, T., Li, J. L., Zhang, L., Jiang, Y., & Gao, F. (2022). Oxidative stress impairs
727 the meat quality of broiler by damaging mitochondrial function, affecting calcium
728 metabolism and leading to ferroptosis. *Animal bioscience, 35*(10), 1616-1627.
729 DeHart, D. N., Fang, D., Heslop, K., Li, L., Lemasters, J. J., & Maldonado, E. N. (2018).
730 Opening of voltage dependent anion channels promotes reactive oxygen species
731 generation, mitochondrial dysfunction and cell death in cancer cells. *Biochemical*
732 *Pharmacology, 148*, 155-162.
733 Goetzman, E. S., Bharathi, S. S., Zhang, Y., Zhao, X.-J., Dobrowolski, S. F., Peasley, K., Sims-
734 Lucas, S., & Monga, S. P. (2020). Impaired mitochondrial medium-chain fatty acid
735 oxidation drives periportal macrovesicular steatosis in sirtuin-5 knockout mice.
736 *Scientific Reports, 10*(1), 18367.
737 Giuliani, KTK., Grivei, A., Nag, P., Wang, X. J., Rist, M., Kildey, K., Law, B., Ng, M. S.,
738 Wilkinson, R., Ungerer, J., Forbes, J. M., Healy, H., & Kassianos, A. J. (2022). Hypoxic
739 human proximal tubular epithelial cells undergo ferroptosis and elicit an NLRP3
740 inflammasome response in CD1c+ dendritic cells. *Cell Death & Disease, 13*(8), 739.
741 Gamage, U. S. K., Hashimoto, S., Miyamoto, Y., Nakano, T., Yamanaka, M., Koike, A., Satoh,
742 M., & Morimoto, Y. (2022). Mitochondria transfer from adipose stem cells improves
743 the developmental potential of cryopreserved oocytes. *Biomolecules, 12*(7), 1008.
744 Guo, M., Zhu, Y. F., Shi, Y., Meng, X. D., Donga, X., Zhang, H. K., Wang, X. H., Du, M., &
745 Yan, H. (2022). Inhibition of ferroptosis promotes retina ganglion cell survival in
746 experimental optic neuropathies. *Redox biology, 58*, 102541.
747 Huang, F., Ding, Z. J., Chen, J. S., Guo, B., Wang, L. L., Liu, C. M., & Zhang, C. H. (2023).

748 Contribution of mitochondria to postmortem muscle tenderization: a review. *Critical*
749 *Reviews in Food Science and Nutrition*, 11-17.
750 Huang, C. Y., Blecker, C., Chen, L., Xiang, C., Zheng, X. C., Wang, Z. Y., & Zhang, D. Q.
751 (2023). Integrating identification and targeted proteomics to discover the potential
752 indicators of postmortem lamb meat quality. *Meat Science, 199,* 109126.
753 Hong, Z. C., Tang, P. L., Liu, B., Ran, C. W., Yuan, C., Zhang, Y., Lu, Y., Duan, X. Y., Yang, Y.
754 F., & Wu, H. Z. (2021). Ferroptosis-related genes for overall survival prediction in
755 patients with colorectal cancer can be inhibited by gallic acid. *International journal of*
756 *biological sciences, 17*(4), 942-956.
757 Hernandez-Garcia, E., Vargas, M., & Torres-Giner, S. (2022). Quality and shelf-life stability of
758 pork meat fillets packaged in multilayer polylactide films. *Foods, 11*(3), 426.
759 Hekimi, S., Wang, Y., & Noe, A. (2016). Mitochondrial ROS and the effectors of the intrinsic
760 apoptotic pathway in aging cells: The discerning killers! *Frontiers in genetics, 7*, 161.
761 Joubert, F., & Puff, N. (2021). Mitochondrial cristae architecture and functions: Lessons from
762 minimal model systems. *Membranes, 11*(7), 465.
763 Javadov, S. (2022). Mitochondria and ferroptosis. *Current Opinion in Physiology,*
764 *25*(prepublish), 100483.
765 Kontchou, C. W., Gentle, I. E., Weber, A., Schoeniger, A., Edlich, F., Häcker, & G. (2022).
766 Chlamydia trachomatis inhibits apoptosis in infected cells by targeting the pro-
767 apoptotic proteins Bax and Bak. *Cell death and differentiation, 29*(10), 2046-2059.
768 Ke, YL., Mitacek, RM., Abraham, A., Mafi, GG., VanOverbeke, DL., & DeSilva,
769 U.Ramanathan, R. (2017). Effects of muscle-specific oxidative stress on cytochrome c

release and oxidation-reduction potential properties. *Journal of agricultural and food chemistry, 65*(35), 7749-7755.

Li, HJ., Chang, LX., Pan, N., Du, X., Shi, S., Zhang, QY., An, GR., Xia, XF., & Zhang, L. (2023). Dynamic changes in postmortem quality of mirror carp (Cyprinus carpio L.): Based on oxidation reaction and mitochondrial function properties. *Food Chemistry, 425*, 136426.

Lei, J. Q., Dong, Y. Y., Hou, Q. H., He, Y., Lai, Y. J., Liao, C. Y., Kawamura, Y., Li, J. Y., & Zhang, B. K. (2022). Intestinal microbiota regulate certain meat quality parameters in chicken. *Frontiers in Nutrition, 9*, 747705.

Liu, C. M., Ding, Z. J., Zhang, Z. H., Zhao, L. Y., Zhang, C. H., & Huang, F. (2023). Morphological changes of mitochondria-related to apoptosis during postmortem aging of beef muscles. *Food Chemistry: X, 19*, 100806.

Liu, J., Hu, Z. Y., Ma, Q., Wang, S. Z., & Liu, D. H. (2023b). Ferritin-dependent cellular autophagy pathway promotes ferroptosis in beef during cold storage. *Food Chemistry, 412*, 135550.

Liu, J. Hu, Z. Y., Ma, Q., Yang, C. Y., Zheng, A. R., & Liu, D. H. (2023a). Reduced water-holding capacity of beef during refrigeration is associated within creased heme oxygenase 1 expression, oxidative stress and ferroptosis. *Meat Science, 202*, 109202.

Liu, J., Liu, D. H., Zheng, A. R., & Ma, Q. (2022). Haem-mediated protein oxidation affects water-holding capacity of beef during refrigerated storage. *Food Chemistry: X, 14*, 100304.

Li, Y. J., Li, J., Li, Z. L., Wei, M. K., Zhao, H. Z., Miyagishi, M., Wu, S. R., & Kasim, V. (2022).

Homeostasis imbalance of YY2 and YY1 promotes tumor growth by manipulating ferroptosis. *Advanced Science (Weinheim, Baden-Wurttemberg, Germany), 9*(13), e2104836.

Li, X., Tu, Z. C., Sha, X. M., Li, Z. Y., Li, J. L., & Huang, M. Z. (2022). Effect of coating on flavor metabolism of fish under different storage temperatures. *Food Chemistry: X, 13*, 100256.

Patinho, I., Cavalcante, C. L., Saldaña, E., Gagaoua, M., Behrens, J. H., & Contreras-Castillo, C. J. (2024). Assessment of beef sensory attributes and physicochemical characteristics: A comparative study of intermediate versus normal ultimate pH striploin cuts. *Food Research International, 175*, 113778.

Park, B. K., Lee, D. K., Ahn, J. S., Park, J. K., Kim, M. J., Son, G. H., & Shin, J. S. (2019). Effects of dietary levels of tapioca residue on growth performance and carcass characteristics in Hanwoo steers. (2019). *Asian-Australasian Journal of Animal Sciences, 32*(8), 1128-1136.

Peoples, J. N., Saraf, A., Ghazal, N., Pham, T. T., & Kwong, J. Q. (2019). Mitochondrial dysfunction and oxidative stress in heart disease. *Experimental & Molecular Medicine, 51*(12), 1-13.

Pongsetkul, J., Siriwong, S., Thumanu, K., Boonanuntanasarn, S., & Yongsawatdigul, J. (2023). Investigating the effect of various sous-vide cooking conditions on protein structure and texture characteristics of tilapia fillet using synchrotron radiation-based FTIR. *Foods, 12*(3), 568.

Paradkar, P. N., Zumbrennen, K. B., Paw, B. H., Ward, D. M., & Kaplan, J. (2009). Regulation

of mitochondrial iron import through differential turnover of mitoferrin 1 and mitoferrin 2. *Molecular and Cellular Biology, 29*(4), 1007-1016.

Rivera, N A., Novakofski, J., Weng, H. Y., Kelly, A., Satterthwaite-Phillips, D., Ruiz, M. O., & Mateus-Pinilla, N. (2015). Metals in obex and retropharyngeal lymph nodes of Illinois white-tailed deer and their variations associated with CWD status. *Prion, 9*(1), 48-58.

Smili, H., Becila, S., della Malva, A., Redjeb, A., Albenzio, M., Sevi, A., Santillo, A., Babelhadj, B., Adamou, A., Boudjellal, A., & Marino, R. (2022). Postmortem muscle protein changes as a tool for monitoring sahraoui dromedary meat quality characteristics. *Foods, 11*(5), 732.

Sebag, S. C., Koval, O. M., Paschke, J. D., Winters, C. J., Comellas, A. P., & Grumbach, I. M. (2018). Inhibition of the mitochondrial calcium uniporter prevents IL-13 and allergen-mediated airway epithelial apoptosis and loss of barrier function. *Experimental Cell Research, 362*(2), 400-411.

Sun, K., Zhi, Y., Ren, W. H., Li, S. M., Zhou, X. Q., Gao, L., & Zhi, K. Q. (2023). The mitochondrial regulation in ferroptosis signaling pathway and its potential strategies for cancer. *Biomedicine & Pharmacotherapy, 169*(2023), 115892.

Shi, W., Zhang, H., Zhang, Y., Lu, L., Zhou, Q., Wang, Y. C., Pu, Y. P., & Yin, L. H. (2023). Co-exposure to Fe, Zn, and Cu induced neuronal ferroptosis with associated lipid metabolism disorder via the ERK/cPLA2/AA pathway. *Environmental pollution (Barking, Essex : 1987), 336*, 122438.

Tang, X. F., Jiang, F., Wang, X. Y., Xia, Y., Mao, Y., & Chen, Y. (2022). Identification of the ferroptosis-related long non-coding RNAs signature to improve the prognosis

prediction in papillary renal cell carcinoma. *Frontiers in Surgery, 9*, 741726.

Van der Reest, J., Lilla, S., Zheng, L., Zanivan, S., & Gottlieb, E. (2018). Proteome-wide analysis of cysteine oxidation reveals metabolic sensitivity to redox stress. *Nature communications, 9*(1), 1581.

Wang, L., Li, J. J., Teng, S., Zhang, W. G., Purslow, P. P., Zhang, R. Y. (2022). Changes in collagen properties and cathepsin activity of beef M. semitendinosus by the application of ultrasound during post-mortem aging. *Meat science,* 185, 108718.

Wang, W. X., Lin, H. X., Guan, W. Q., Song, Y., He, X. X., & Zhang, D. Q. Effect of static magnetic field-assisted thawing on the quality, water status, and myofibrillar protein characteristics of frozen beef steaks. *Food Chemistry, 436*, 137709.

Wang, L. L., Yu, Q. L., Han, L., Ma, X. L., Song, R. D., Zhao, S. N., & Zhang, W. H. (2018). Study on the effect of reactive oxygen species-mediated oxidative stress on the activation of mitochondrial apoptosis and the tenderness of yak meat. *Food Chemistry, 244*, 394-402.

Xin, K. Q., Tian, K., Yu, Q. L., Han, L. (2023). High oxygen-modified packaging (HiOx-MAP) mediates HIF-1α regulation of tenderness changes during postmortem aging of yak meat. *Food Chemistry: X, 2023*(17), 100573.

Xie, Y. H., Mei, X. Y., & Shi, W. M. (2023). Kaempferol promotes melanogenesis and reduces oxidative stress in PIG1 normal human skin melanocytes. *Journal of cellular and molecular medicine, 27*(7), 982-990.

Xue, X. F., Ma, L. F., Zhang, X., Xu, X., Guo, S. S., Wang, Y. K., Qiu, S. Y., Cui, J. T., Guo, W. X., Yu, Y. C., Sun, F. Y., Shi, Y., & Wang, J. Y. (2022). Tumour cells are sensitised to

ferroptosis via RB1CC1-mediated transcriptional reprogramming. *Clinical and Translational Medicine, 12*(2), e747.

Yu, Q. Q., Tian, X. J., Shao, L. L., Li, X. M., & Dai, R. T. (2020). Mitochondria changes and metabolome differences of bovine longissimus lumborum and psoas major during 24 h postmortem. *Meat Science, 166*, 108112.

Yagoda, N., von Rechenberg, M., Zaganjor, E., Bauer, A. J., Yang, W. S., Fridman, D. J., Wolpaw, A. J., Smukste, I., Peltier, J. M., Boniface, J. J., Smith, R., Lessnick, S. L., Sahasrabudhe, S., & Stockwell, BR. (2007). RAS-RAF-MEK-dependent oxidative cell death involving voltage-dependent anion channels. *Nature, 447*(7146), 864-868.

Zou, B., Shao, LL., Yu, QQ., Zhao, YJ., Li, XM., & Dai, RT. (2022). Changes of mitochondrial lipid molecules, structure, cytochrome c and ROS of beef Longissimus lumborum and Psoas major during postmortem storage and their potential associations with beef quality. *Meat Science, 195*, 109013.

Zhang, B. Y., Sun, Z. Q., Yu, Z., Li, H. H., Luo, H. L., & Wang, B. (2022). Transcriptome and targeted metabolome analysis provide insights into bile acids' new roles and mechanisms on fat deposition and meat quality in lamb. *Food Research International, 2022, 162* (PA), 111941.

Zhang, W. F., Gong, M. Y., Zhang, W. N., Mo, J. T., Zhang, S. M., Zhu, Z., Wang, X. N., Zhang, B. Qian, W. K., Wu, Z., Ma, Q. Y., & Wang, Z. (2022). Thiostrepton induces ferroptosis in pancreatic cancer cells through STAT3/GPX4 signalling. *Cell Death & Disease, 13*(7), 630.

Zhang, W. Q., Lu, J. H., Wang, Y. Y., Sun, P. B., Gao, T., Xu, N. H., Zhang, Y. U., & Xie, W. D.

(2023). Canagliflozin attenuates lipotoxicity in cardiomyocytes by inhibiting inflammation and ferroptosis through activating AMPK pathway. *International Journal of Molecular Sciences, 24*(1), 858.

Zhang, J. Y., Ma, G. Y., Guo, Z. B., Yu, Q. L., Han, L., Han, M. S., & Zhu, Y. M. (2018). Study on the apoptosis mediated by apoptosis-inducing-factor and influencing factors of bovine muscle during postmortem aging. *Food Chemistry, 266*, 359-367.

Zhang, H. P., Tang, D. B., Yang, H. G., Liu, X. M., Cheng, J. R., Wang, X. P., Zou, J. H., & Lin, Y. S. (2023). Effects of high hydrostatic pressure assisted enzymatic tenderization on goose meat texture and myofibril protein. *LWT, 184,* 114845.

Zhang, Z., Xia, G. H., Yang, Q., Fan, X. W., & Lyu, S, X. (2019). Effects of chitosan-based coatings on storage quality of Chinese shrimp. *Food Science & Nutrition, 7*(12), 4085-4094.

Zhou, L., Yu, P., Wang, T. T., Du, Y. W., Chen, Y., Li, Z., He, M. L., Feng, L., Li, H. R., Han, X., Ma, H., & Liu, H. B. (2022). Polydatin attenuates cisplatin-induced acute kidney injury by inhibiting ferroptosis. *Oxidative Medicine and Cellular Longevity, 2022*, 9947191.

Zhou, J. W., Zhang, Y., Wu, J. J., Qiao, M., Xu, Z., Peng, X. W., & Mei, S. Q. (2021). Proteomic and lipidomic analyses reveal saturated fatty acids, phosphatidylinositol, phosphatidylserine, and associated proteins contributing to intramuscular fat deposition. *Journal of Proteomics, 241*, 104235.

Zhang, R. Y., Zhang, J., Zhou, L., Wang, L., & Zhang, W. G. (2021). Influence of ultrasound-assisted tumbling on NaCl transport and the quality of pork. *Ultrasonics Sonochemistry,*

902 *79*, 105759.

903

Figures captions

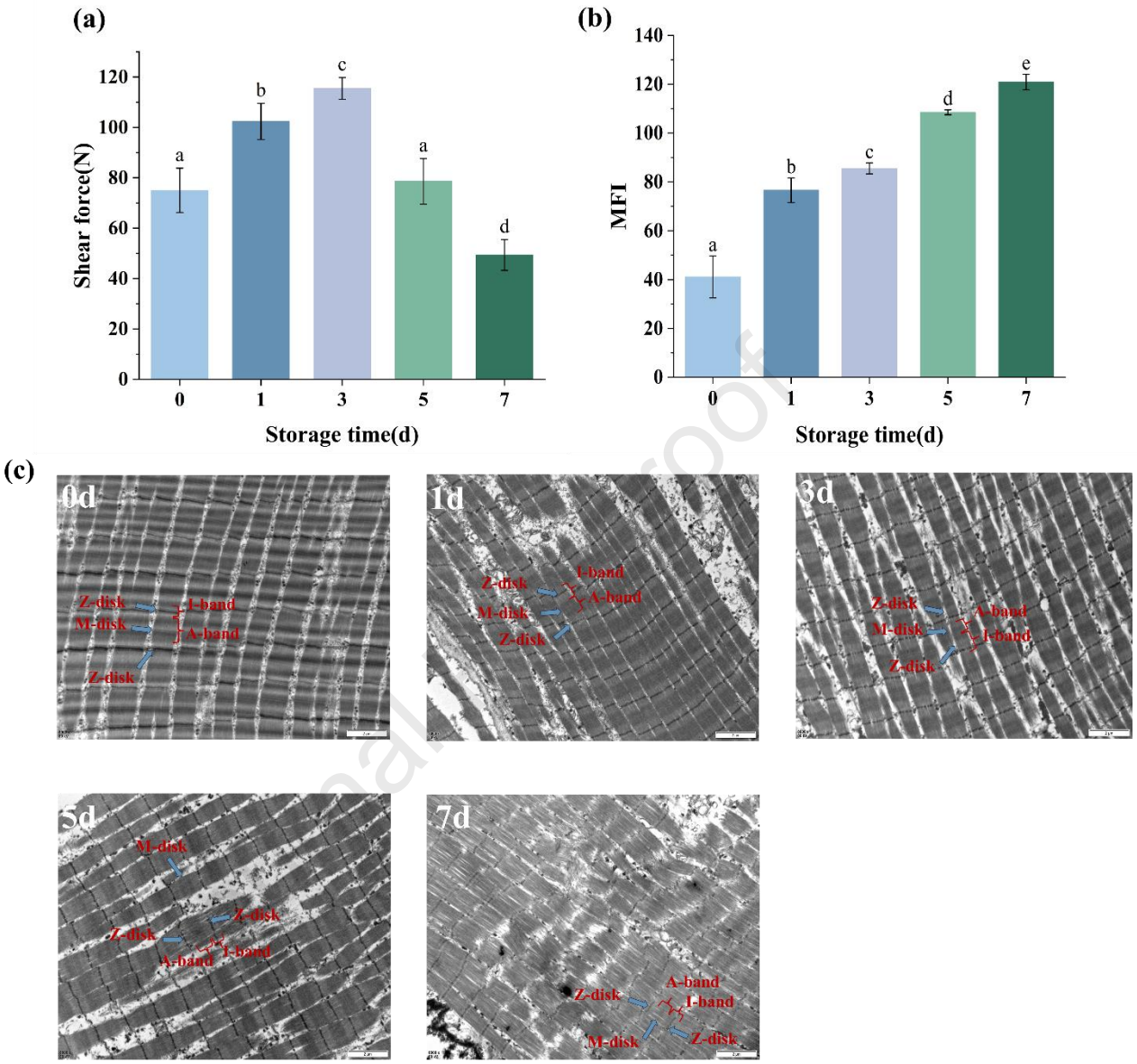

Fig.1. Change in the tenderness of beef meat during refrigeration; (a) Shear force of beef meat during refrigeration; (b) MFI of beef meat during refrigeration; (c) Myofibrillar microstructure of beef meat during refrigeration. Scale bar = 0.2 μm. Different superscript letters represent statistically significant differences (p<0.05).

Table 1 Texture profile of beef meat during refrigeration

Storage time (d)	0	1	3	5	7
Hardness (N)	40.50±10.14^{ab}	31.10±6.85^{a}	60.27±14.16^{b}	48.37±20.65^{ab}	33.77±2.47^{a}
Chewiness (mJ)	70.47±13.78^{ab}	51.07±14.64^{a}	100.09±7.45^{b}	74.06±30.50^{ab}	67.51±5.87^{a}
Cohesiveness (Ratio)	0.60±0.02^{a}	0.59±0.01^{a}	0.62±0.00^{a}	0.54±0.05^{b}	0.58±0.03^{ab}
Springiness (mm)	3.21±0.17^{ab}	2.74±0.25^{a}	3.40±0.56^{b}	2.88±0.25^{ab}	3.06±0.31^{ab}

Note: Values in the same row with different superscript letters represent statistically significant differences (p<0.05).

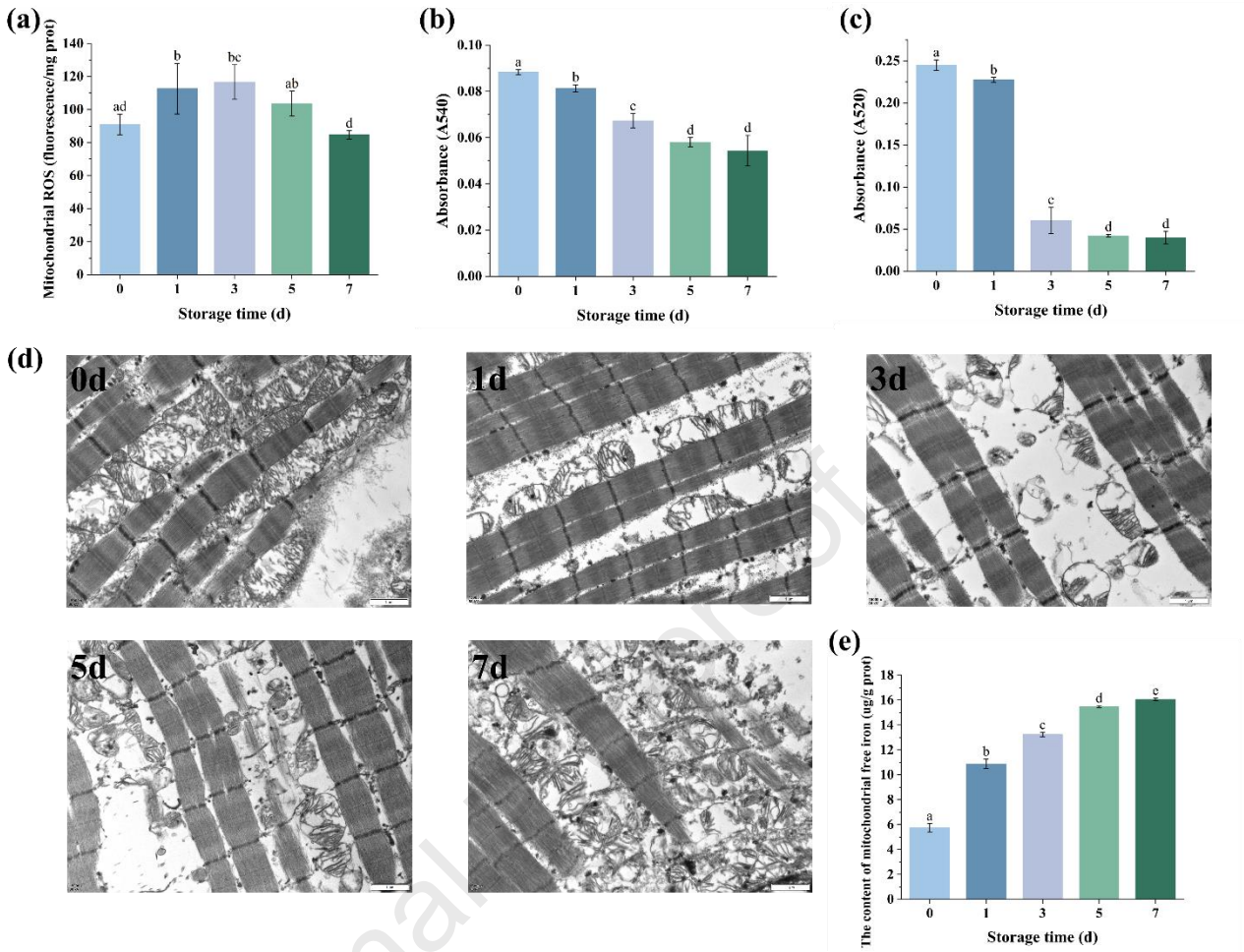

Fig.2. The extent of mitochondrial damage in beef. (a) Mitochondrial ROS level during refrigeration; (b) MPTP during refrigeration; (c) Mitochondrial swelling during refrigeration; (d) Ultrastructure of intermyofibrillar mitochondria during refrigeration, scale bar = 0.1 μm; (e) The contents of mitochondrial free iron during refrigeration.

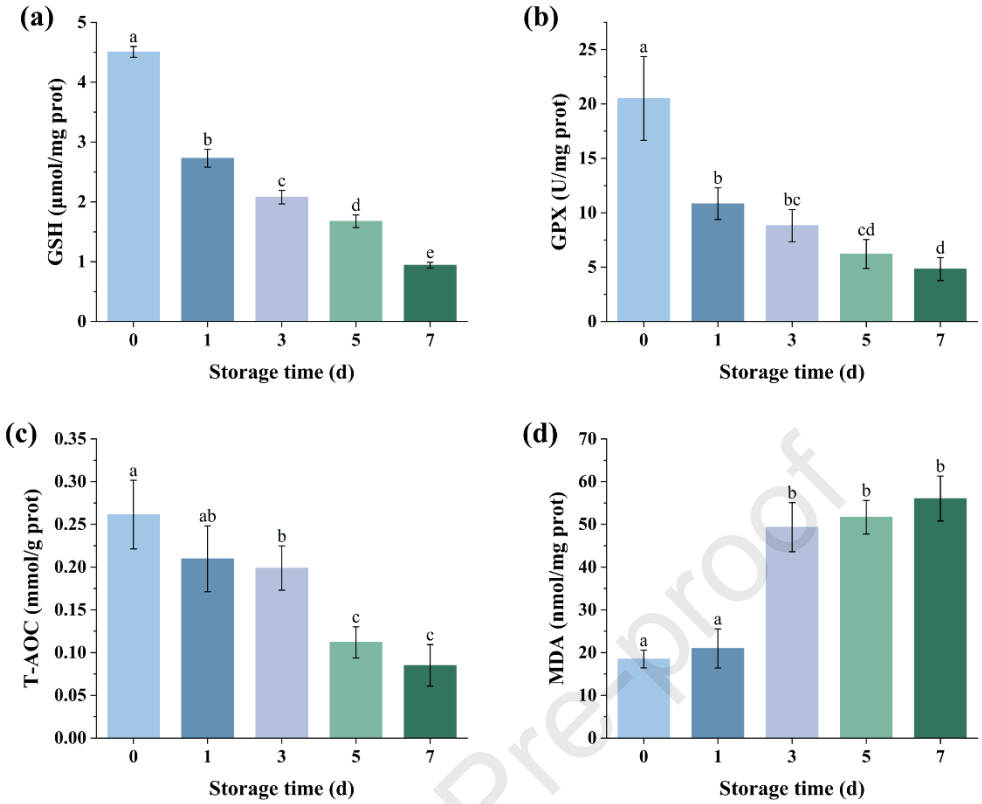

Fig.3. Mitochondrial antioxidant capacities. (a) Mitochondrial GSH content during refrigeration; (b) GPX activity during refrigeration; (c) Mitochondrial T−AOC during refrigeration; (d) Mitochondria MDA content during refrigeration.

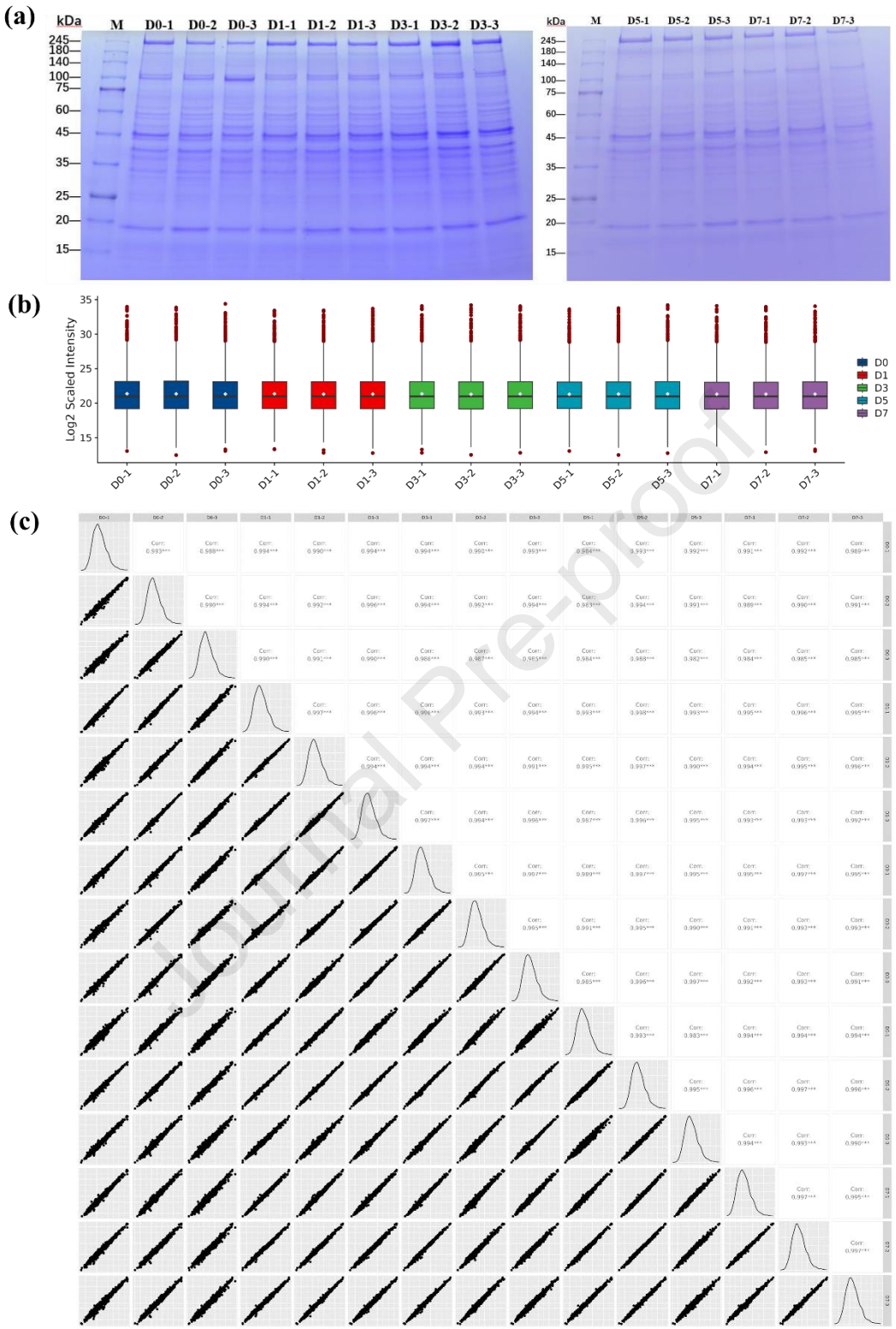

925
926 **Fig.4.** (a) SDS-PAGE analysis; (b) Boxplot of protein expression level; (c) Sample correlation
927 diagram.

928

929

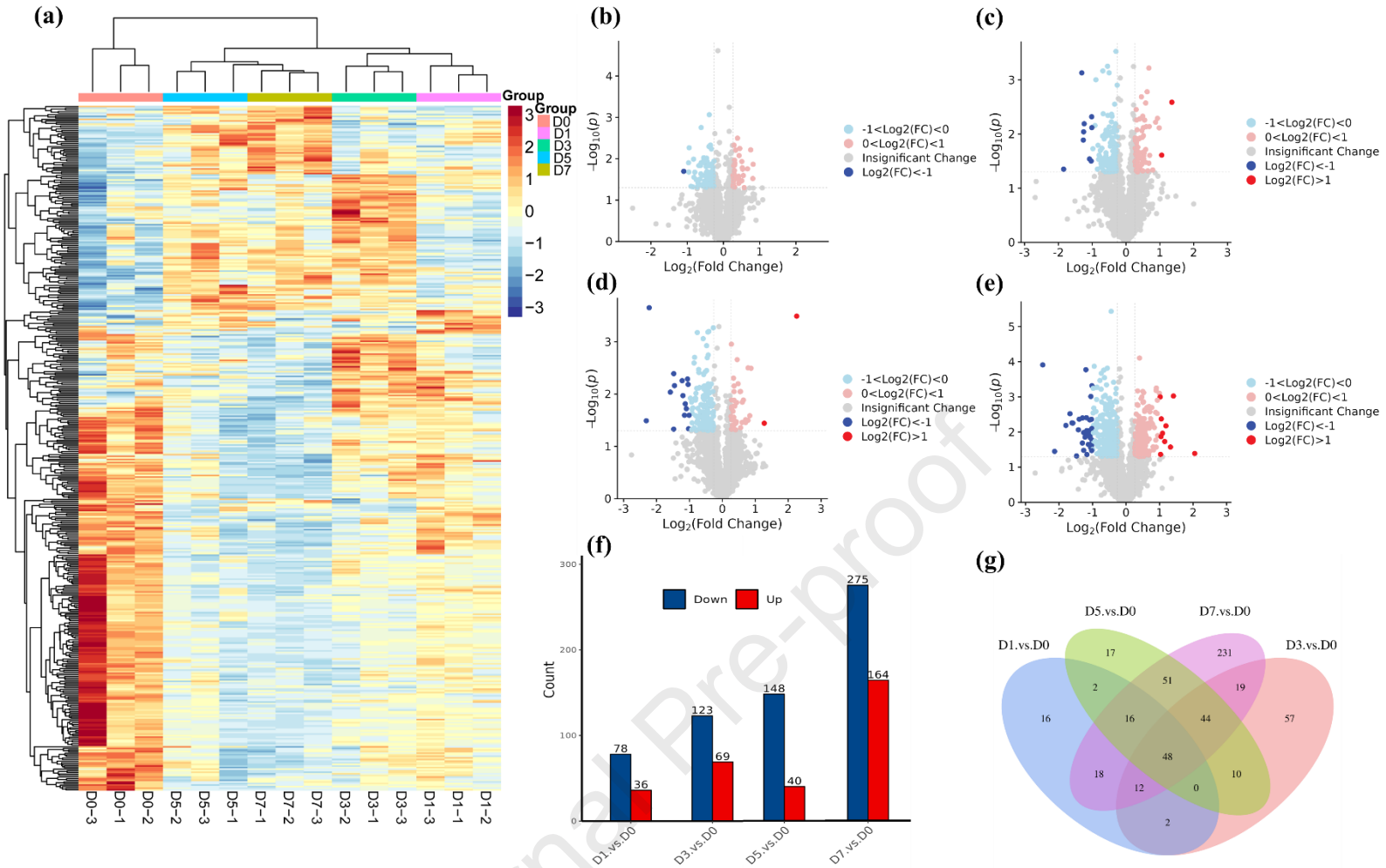

Fig.5. (a) Hierarchical clustering analysis heatmap of differentially expressed proteins (DEPs); (b) Volcano plot of the DEPs between 1 d and 0 d; (c) Volcano plot of the DEPs between 3 d and 0 d; (d) Volcano plot of the DEPs between 5 d and 0 d; (e) Volcano plot of the DEPs between 7 d and 0 d; (f). Numbers of DEPs in each pairwise comparison; (g) Venn plot of DEPs in each pairwise comparison.

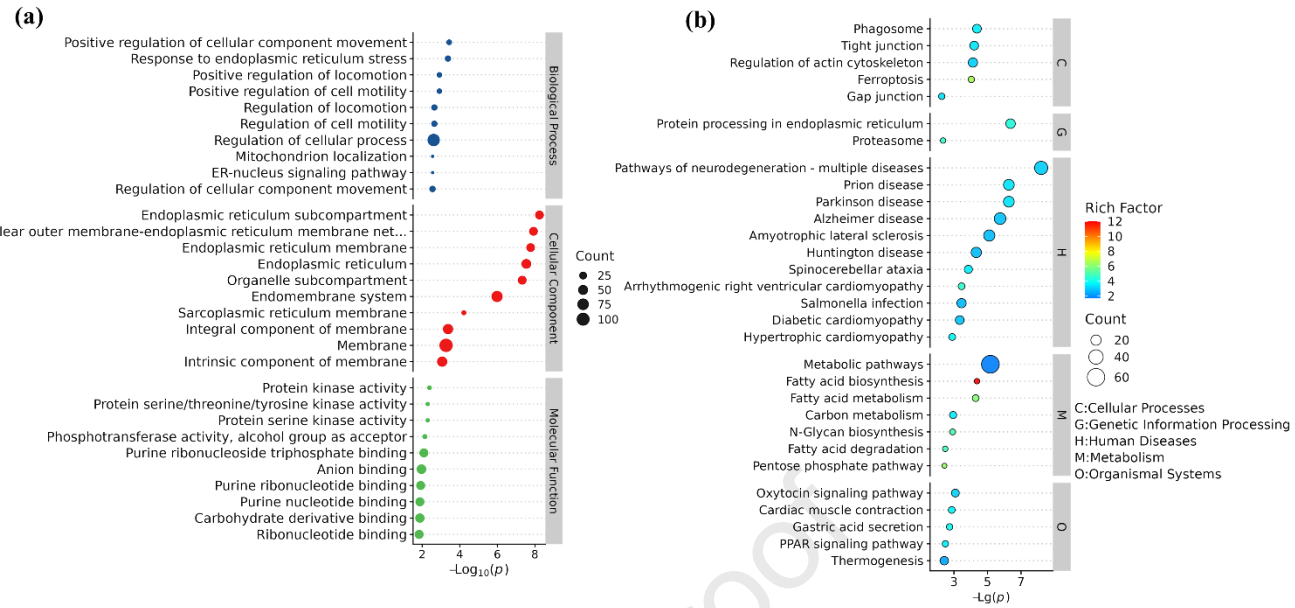

Fig.6. (a) GO functional enrichment bubble plot of DEPs; (b) KEGG pathway enrichment bubble plot of DEPs.

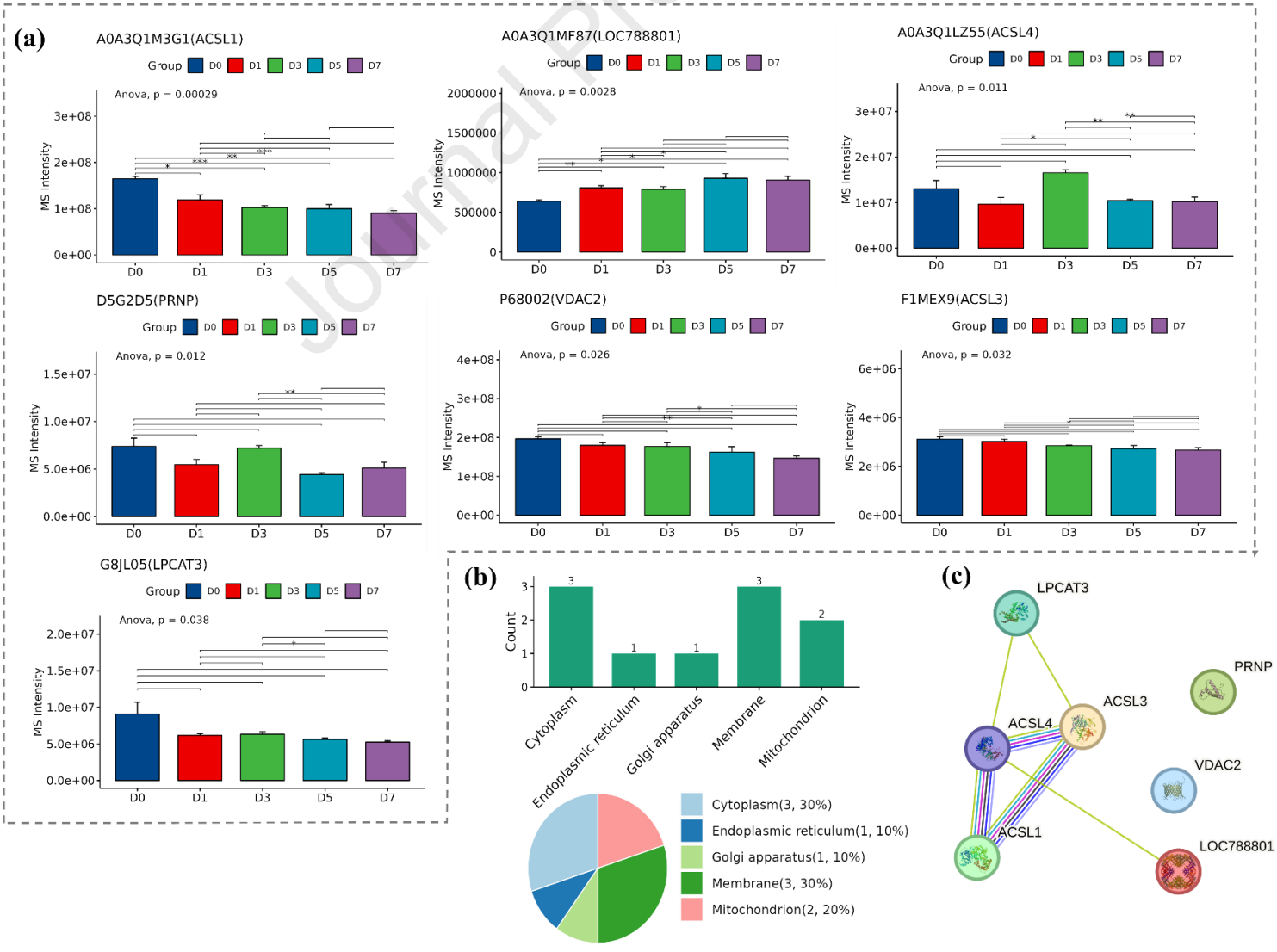

Fig.7. (a) Changes in MS intensity of DEPs enriched into the ferroptosis pathway; (b) Subcellular localization of DEPs enriched into the ferroptosis pathway; (c) Protein–protein interaction (PPI) network enriched into the ferroptosis pathway.

Table 2 PRM verification

Number	Gene name	Unioort ID	Peptide sequence	Relative abundance of peptide				
				Log_{10} 0d	Log_{10} 1d	Log_{10} 3d	Log_{10} 5d	Log_{10} 7d
1	VDAC2	P68002	VNNSSLIGVGYTQTLRPGVK	7.569±0.013	7.673±0.061	7.343±0.037	7.361±0.069	7.108±0.010
2	ACSL1	A0A3Q1M3G1	IFGQANTTLK	6.943±0.019	6.936±0.017	6.611±0.014	6.585±0.036	6.449±0.099
3	LPCAT3	G8JL05	SLTSEQQIYAIR	6.817±0.015	6.788±0.049	6.540±0.037	6.497±0.040	6.075±0.024
4	VDAC3	A6H783	LTLDTIFVPNTGK	8.544±0.015	8.521±0.023	8.468±0.056	8.464±0.077	8.478±0.035
5	TF	G3X6N3	TSDANIND5NNLK	8.226±0.088	8.259±0.036	8.217±0.022	8.293±0.094	8.331±0.024
6	TFRC	E1BIG6	ILNVFGVIK	7.137±0.006	7.145±0.046	7.155±0.021	7.116±0.035	7.125±0.044
7	PCBP1	Q5E9A3	IITLTGPTNAIFK	7.469±0.035	7.525±0.011	7.467±0.018	7.497±0.024	7.471±0.027
8	CP	A0A3Q1MI22	DIFTGLIGPMK	6.655±0.013	6.715±0.047	6.693±0.011	6.754±0.087	6.762±0.015
9	PCBP2	Q3SYT9	IANPVEGSTDR	6.036±0.023	6.114±0.036	6.067±0.019	6.071±0.038	6.049±0.045
10	ACADM	Q3SZB4	TGEYPVPLIK	6.220±0.050	6.401±0.023	6.327±0.026	6.309±0.040	6.629±0.049

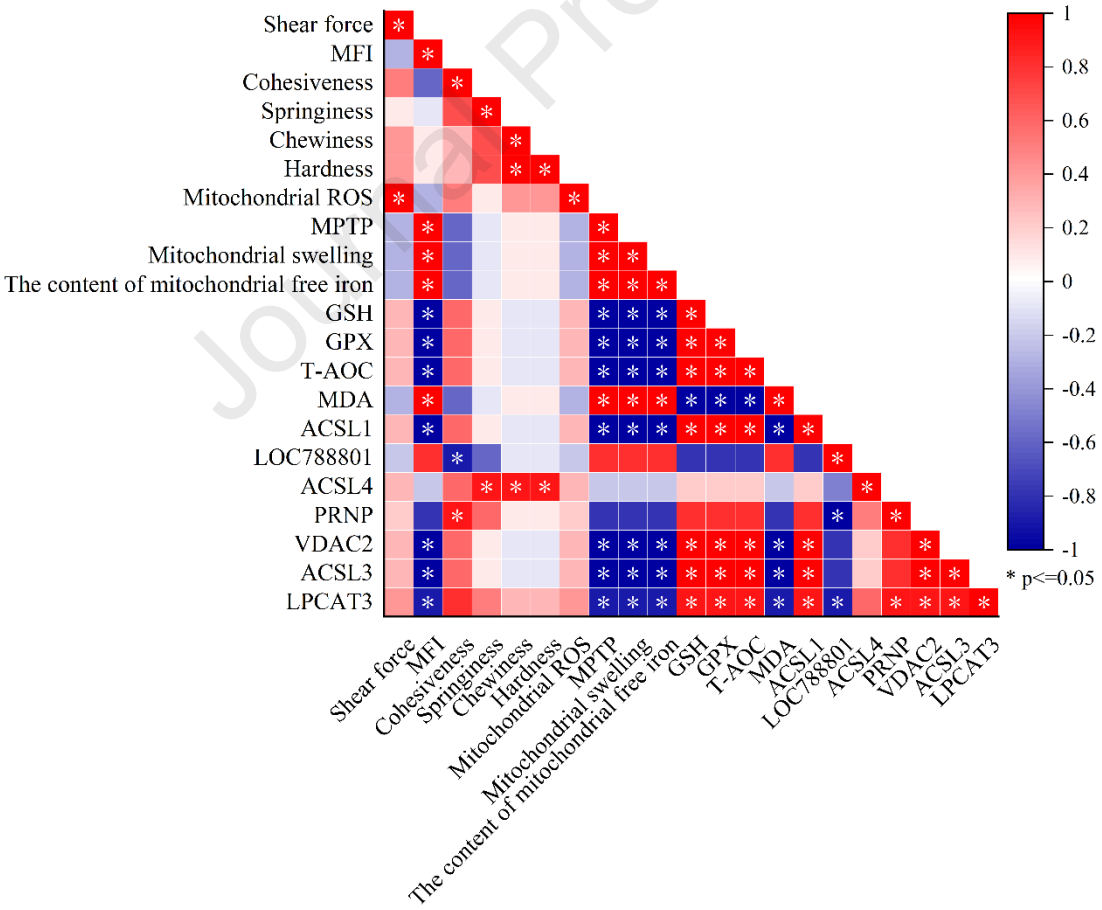

Fig.8. Correlation matrix heat map between mitochondrial oxidative stress-mediated beef ferroptosis and tenderness during refrigeration.

Highlights

- Mitochondrial oxidative stress-mediated ferroptosis promoted beef tenderization.
- Beef mitochondria showed oxidative stress and typical ferroptosis characteristics.
- Lipid metabolism was the main mitochondrial pathway involved in ferroptosis.

Declaration of interests

The authors declare that they have no known competing financial interests or personal relationships that could have appeared to influence the work reported in this paper.